



# A one-photon endoscope for simultaneous patterned optogenetic stimulation and calcium imaging in freely behaving mice

Jinyong Zhang<sup>1</sup>, Ryan N. Hughes<sup>1</sup>, Namsoo Kim<sup>1</sup>, Isabella P. Fallon<sup>2</sup>, Konstantin Bakhurin<sup>1</sup>, Jiwon Kim<sup>1</sup>, Francesco Paolo Ulloa Severino<sup>1,3</sup> and Henry H. Yin<sup>1,2</sup>✉

**Optogenetics and calcium imaging can be combined to simultaneously stimulate and record neural activity *in vivo*. However, this usually requires two-photon microscopes, which are not portable nor affordable. Here we report the design and implementation of a miniaturized one-photon endoscope for performing simultaneous optogenetic stimulation and calcium imaging. By integrating digital micromirrors, the endoscope makes it possible to activate any neuron of choice within the field of view, and to apply arbitrary spatiotemporal patterns of photostimulation while imaging calcium activity. We used the endoscope to image striatal neurons from either the direct pathway or the indirect pathway in freely moving mice while activating any chosen neuron in the field of view. The endoscope also allows for the selection of neurons based on their relationship with specific animal behaviour, and to recreate the behaviour by mimicking the natural neural activity with photostimulation. The miniaturized endoscope may facilitate the study of how neural activity gives rise to behaviour in freely moving animals.**

A major technological advance in neuroscience is the ability to record and manipulate neural activity with light. Readout of neural activity is made possible by the development of genetically encoded calcium indicators that bind to intracellular calcium and emit fluorescence that is proportional to neural activity<sup>1</sup>. Manipulation of neural activity can be achieved by optogenetics, using different genetically expressed light-sensitive ion channels (opsins) to activate and inactivate specific neuronal populations<sup>2,3</sup>. Together, these techniques have revolutionized neuroscience, allowing investigators to record and manipulate neural activity with cell type specificity in behaving animals<sup>4–7</sup>.

More recently, calcium imaging and optogenetics have been combined in 2-photon (2P) microscopy to manipulate and image neural activity at the same time<sup>8–12</sup>. With this ‘all-optical’ approach, the same neurons can be recorded and stimulated simultaneously, and light delivery can be restricted to individual neurons. It is also possible to mimic normal neural activity by replaying the activity from calcium imaging using more physiologically realistic stimulation parameters<sup>13–16</sup>. Currently, 2P microscopy is the gold standard for all-optical stimulation and recording at cellular resolution<sup>9,13,17</sup>. However, traditional 2P microscopy has key limitations such as high cost and lack of portability, making it difficult to use in freely moving animals. Although recent work has developed a portable 2P system, it is still not possible to combine patterned stimulation and calcium imaging simultaneously<sup>18</sup>. While 1-photon (1P) patterned stimulation and imaging systems have also been developed<sup>19–22</sup>, they also have considerable limitations, such as the need for a benchtop confocal microscope that limits system portability.

To overcome these limitations, we developed a 1P system for simultaneous stimulation and calcium imaging—the Miniscope with All-optical Patterned Stimulation and Imaging (MAPSI). MAPSI integrates pattern stimulation and calcium recording in a single system with a small body (25 mm × 15 mm × 15 mm).

It makes it possible to mimic natural physiological patterns just recorded, instead of delivering artificial stimulation patterns to all neurons expressing opsins indiscriminately. Neural activity can be recorded and analysed in real-time while selecting and stimulating neurons that are behaviourally relevant. MAPSI thus makes it possible to perform closed-loop experiments in which neural activity is maintained or shaped online.

## Results

**Design of MAPSI.** The calcium imaging component in MAPSI is based on the UCLA Miniscope, which allows imaging of many neurons in freely moving animals<sup>23</sup>. To integrate light-emitting diode (LED) excitation of calcium indicators and laser stimulation, we modified the original Miniscope design to incorporate a digital micromirror device (DMD) and an additional laser light source. DMDs can create arbitrary light patterns with extremely high spatial and temporal resolution. They have been used for photostimulation *in vitro*<sup>20,24</sup> and *in vivo*<sup>22,25</sup>. To record and stimulate simultaneously, we used two light sources: the first is a lime LED (540 nm–580 nm filter) for excitation of calcium indicators. This LED is controlled by a constant current source capable of producing up to 200 mA with a step size of 4 mA, with up to 12 mW mm<sup>-2</sup> measured beneath the gradient-index (GRIN) lens (Supplementary Fig. 1). The second light source is an external laser (Opto Engine, PSU-H-LED) that generates blue light for optogenetic excitation (473 nm). By passing the excitation light through the DMD<sup>24,26</sup>, we could generate a patterned light beam, which is merged with the excitation light for calcium imaging in the main excitation path (Fig. 1). The DMD is controlled by a display controller (DLP3430) that can connect to any computer through a High-Definition Multimedia Interface (HDMI) interface board (Supplementary Fig. 1). The orientation of the micromirrors can be precisely controlled by a computer to create different stimulation patterns and sequences. It can be

<sup>1</sup>Department of Psychology and Neuroscience, Duke University, Durham, NC, USA. <sup>2</sup>Department of Neurobiology, Duke University School of Medicine, Durham, NC, USA. <sup>3</sup>Department of Cell Biology, Duke University School of Medicine, Durham, NC, USA. ✉e-mail: hy43@duke.edu

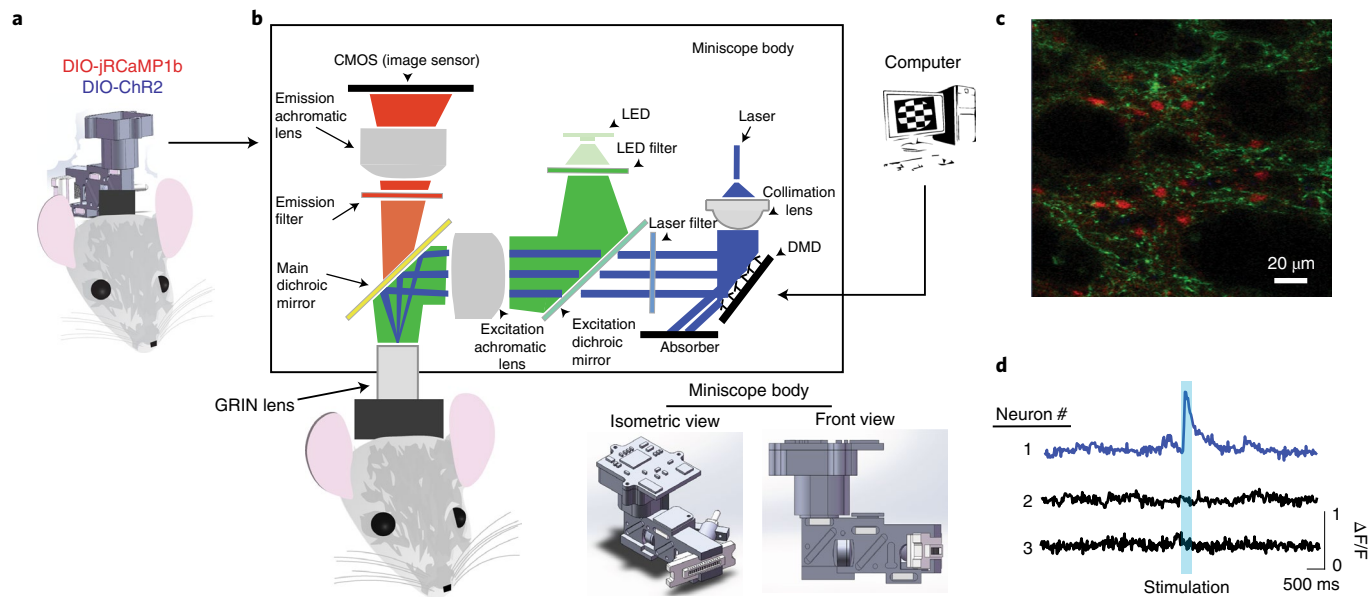


**Fig. 1 | Miniscope with all-optical patterned stimulation and imaging (MAPSI).** **a**, Drawing of MAPSI on a mouse head. jRCaMP1b, a red shifted calcium indicator, was used for imaging and ChR2 for optogenetics. **b**, Schematic of MAPSI components. Two light sources are in the excitation path: the lime LED excites jRCaMP1b and the blue laser light excites ChR2. Micromirrors on the DMD reflect a collimated laser beam, generating arbitrary stimulation patterns created and controlled by a computer. The focal plane of the excitation achromatic lens matches the GRIN lens focal plane to ensure high resolution. The emission path records calcium activity with a CMOS sensor. **c**, Histological image showing dSPNs (D1-cre mouse) that co-express jRCaMP1b and ChR2. **d**, Calcium transients showing excitation of stimulated neuron #1, but not of nearby neighbouring neurons #2 and #3.

programmed to split the collimated light from the laser into individual beams, allowing the experimenter to select and stimulate extremely small areas (Fig. 2 and Supplementary Fig. 2). In the DMD off-state, an absorber is used to avoid light dispersion into the excitation path.

To obtain high resolution, the key challenge is to produce almost perfectly collimated light (<1% deviation). We first simulated our design in optic tracing software (Supplementary Fig. 3). In the main excitation light path, the focal planes of the achromatic lens and the GRIN lens are matched so that the light will precisely target specific regions beneath the GRIN lens. With this collimated beam, photo-stimulation can maintain its precise beamlets with high resolution even after traversing long distances (20 mm) through the excitation path and the GRIN lens.

Because MAPSI is heavier than a conventional miniscope (~7.8 g compared with ~4 g), to help mice carry it, we developed a commutator with a pulley to reduce the weight carried by 4 g, thus allowing free movement for long periods (Supplementary Video 1). A direct comparison of the original UCLA Miniscope and MAPSI in the same animal moving in an open-field arena is shown in Extended Data Fig. 1. In the future, the weight can be further reduced by using a wireless DMD connector and a smaller complementary metal-oxide-semiconductor (CMOS).

**Functional capabilities of MAPSI.** To test the ability of MAPSI to simultaneously stimulate and record neurons in freely moving animals, we injected both viral vectors containing Cre-dependent jRCaMP1b and ChR2-eYFP in the dorsolateral striatum (DLS)<sup>2,27</sup>. jRCaMP1b can be excited by a lime LED with a 540–580 nm excitation filter, and ChR2 can be activated using an excitation wavelength of 473 nm with a 450–490 nm emission filter from a separate laser generator. Using Cre-dependent viral vectors (AAV1-CAG-Flex-jRCaMP1b and AAV5-EF1aa-DIO-hChR2-eYFP) in D1-Cre and A2A-Cre mice, we expressed jRCaMP1b and ChR2-eYFP in direct (D1+) and indirect (A2A+) pathway neurons<sup>28</sup>.

MAPSI was first tested in anaesthetized mice to validate that the stimulation area was similar to the calcium imaging region (Fig. 2a). A baseplate was used to fix MAPSI on the mouse head. More neurons can be recorded and stimulated by re-baseplating to cover another region beneath the GRIN lens. Using a 1.8 mm GRIN lens, the field of view (FOV) is circular, with a diameter of ~250 μm. The power density is 2 mW mm<sup>-2</sup> for imaging excitation and 60–80 mW mm<sup>-2</sup> for optogenetic stimulation. The power density for optogenetic stimulation is similar to what is commonly used in the field (usually 40–200 mW mm<sup>-2</sup>)<sup>29,30</sup>. It has been shown that unacceptable tissue heating is possible with prolonged stimulation at a higher power of >100 mW mm<sup>-2</sup> (>3 mW light from a fibre with 200 μm diameter)<sup>30</sup>. In MAPSI, with a spot 10 μm in diameter for single-neuron stimulation, the power is ~60–80 mW mm<sup>-2</sup>, which is unlikely to create considerable tissue heating.

**Axial and lateral resolution.** To determine the axial (z axis) resolution of MAPSI, we first recorded fluorescence signals from a 200 μm brain slice from a D1-Cre mouse infected with ChR2 and RCaMP1b using a confocal microscope while simultaneously stimulating neurons using MAPSI. The axial resolution and depth of penetration are shown in Fig. 2b. We found that the full-width half-maximum (FWHM) of the stimulation beamlets is approximately 30 μm. The same experiment was also performed in a brain slice from an A2A-Cre mouse, with similar results.

When the laser spot is 10 μm in diameter, the fluorescence detected was almost circular, with 10.5 μm FWHM on the x axis and 9.8 μm FWHM on the y axis (Fig. 2c). The fluorescence linearly increased as the diameter of the illuminated area increased and the intensity decreased as the beamlets penetrated more deeply into the tissue (Fig. 2d). To identify which neurons co-expressed both ChR2 and jRCaMP1b, the jRCaMP1b was continuously excited at low power (~1 mW mm<sup>-2</sup>) to achieve a stable baseline, and ChR2 was excited at 20 Hz (20 ms pulse duration, 20 pulses, power density ~50 mW mm<sup>-2</sup>). During stimulation, we were able to measure a significant increase in jRCaMP1b fluorescence signal by targeting

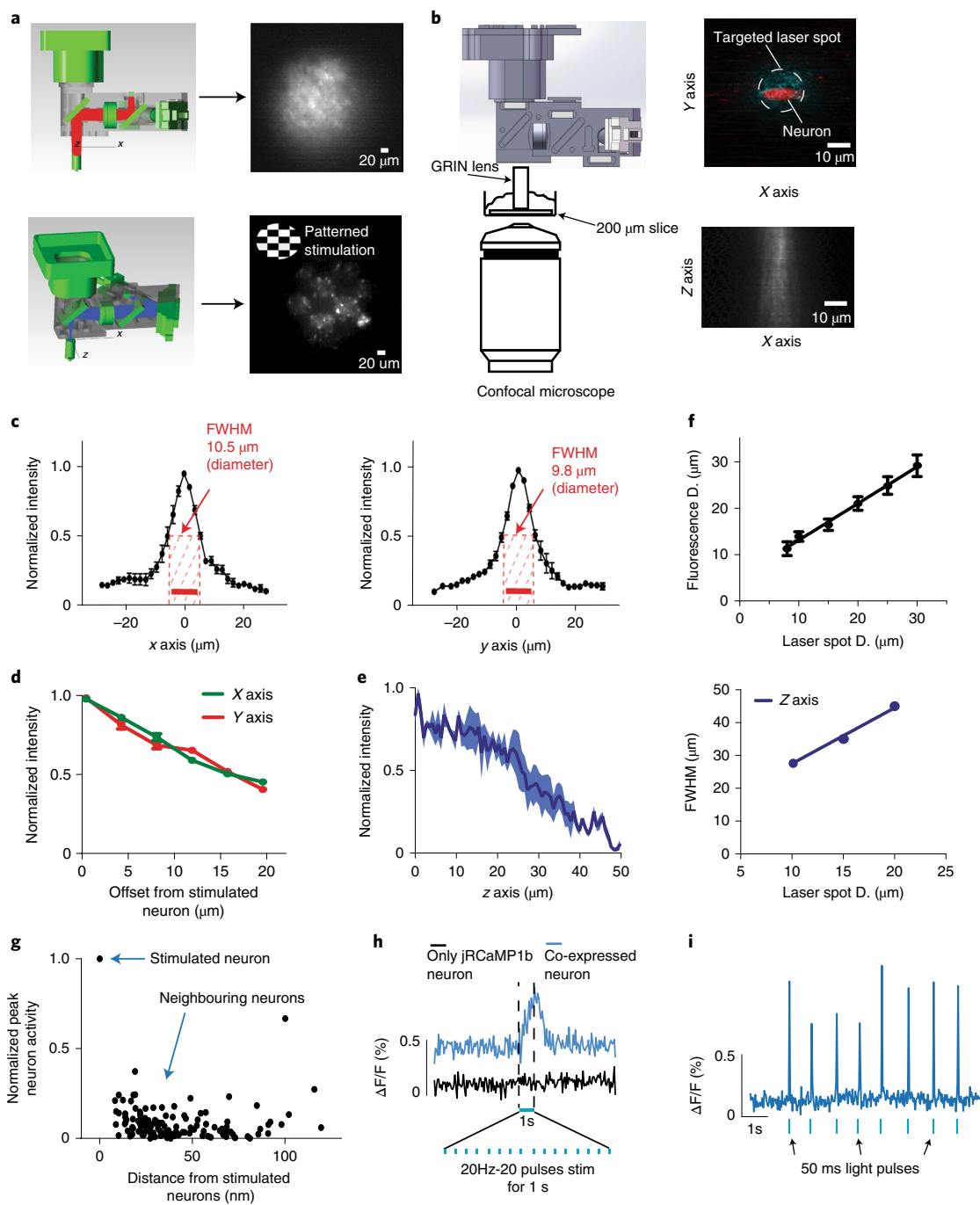


**Fig. 2 | High resolution of MAPSI allows patterned stimulation and calcium imaging.** **a**, Left, schematics of the LED excitation path. Right, field of view (FOV,  $\sim 250 \mu\text{m}$ ). The image is from the mouse striatum, showing D1+ neurons. A checkered illumination pattern was used in the bottom right panel of the patterned optogenetic excitation path. Left: schematic of the setup to validate axial ( $z$  axis) resolution. Right: resolution of stimulated beamlets on the  $x$ - $y$  plane and  $x$ - $z$  plane using a confocal microscope. **c**, Lateral (x (left) and y (right)) resolution. The FWHM of fluorescence ( $N=6$  mice) is less than  $10.5 \mu\text{m}$  on the x axis and  $9.8 \mu\text{m}$  on the y axis using a  $10 \mu\text{m}$  diameter spot. **d**, Fluorescence intensity decreases as a function of laser spot offset. **e**, Axial (z axis) resolution. Left: light intensity along the z axis using a  $10 \mu\text{m}$  diameter laser beamlet (power =  $70 \text{ mW mm}^{-2}$ ,  $n=6$  stimulated neurons). Right: FWHM of the photoactivation beam linearly increases with the spot diameter. **f**, There is a linear relationship between fluorescence diameter and the laser beam diameter ( $D$ ). The minimum fluorescence diameter is  $10 \mu\text{m}$ . **g**, Peak fluorescence of all recorded neurons as a function of distance from the stimulation location (0–500 ms after stimulation onset, 5 mice, 132 neurons, power =  $70 \text{ mW mm}^{-2}$ ). **h**, Comparison of signals from an SPN co-expressing both calcium indicator and opsin and an SPN expressing only the calcium indicator. **i**, A representative stimulated neuron showing reliable responses to stimulation. All error bars indicate s.e.m.

the neuron using a  $10 \mu\text{m}$  diameter spot (Fig. 2d, 31 neurons in 6 mice; all traces are shown in Supplementary Fig. 4). In the absence of ChR2 expression, no fluorescence change was detected (Fig. 2e; 21 cells from 4 control mice with only jRCaMP1b expression).

**Testing in freely moving mice.** MAPSI makes it possible to select individual neurons that are active during behaviours of experimental interest and play back their activity. We used Cre-dependent viral vectors and Cre driver lines to target either the direct pathway

(striatonigral, D1-cre) or the indirect pathway (striatopallidal, A2A-cre)<sup>31–33</sup>. These two well-established pathways are known to have opposite effects on basal ganglia output and behaviour<sup>34–37</sup>. In particular, stimulation of direct pathway spiny projection neurons (dSPNs) can produce contraversive turning behaviour (away from the side of stimulation, towards the contralateral side), and stimulation of indirect pathway spiny projection neurons (iSPNs) can produce ipsiversive turning behaviour (towards the side of stimulation)<sup>34</sup>. Thus, optogenetic manipulation of these pathways provides convenient behavioural readouts to test the efficacy of our all-optical stimulation/imaging system.

To mimic naturally occurring neural activity patterns, we identified neurons that were active during a behaviour of interest. If they co-expressed both ChR2 and jRCaMP1, we could then optogenetically stimulate these neurons while recording their activity (Extended Data Fig. 1).

We tested MAPSI in D1-Cre mice or A2A-Cre mice with a chronically implanted GRIN lens (1.8 mm diameter, 4.3 mm length) during freely moving behaviour. We generated multiple 10 μm beamlets (5 beamlets at 80 mW mm<sup>-2</sup> for dSPNs, 4 beamlets at 60 mW mm<sup>-2</sup> for iSPNs) for stimulation while recording calcium activity from all neurons in the FOV. Individual dSPNs or iSPNs could be robustly and selectively activated without activating neighbouring neurons (Fig. 3, and Extended Data Figs. 2 and 3). Occasionally, a non-stimulated neuron (such as neuron 6 in Fig. 3c) located close to a stimulated neuron (neuron 1 in Fig. 3c) responded almost systematically but with a longer latency (Fig. 3d). This suggests that some neurons can be activated indirectly by stimulation via circuit connections.

**Isolating behaviourally active neurons and manipulating their activity.** To examine the effects of direct pathway activation, we injected Cre-dependent jRCaMP1b and ChR2-eYFP into D1-Cre mice ( $N=3$  mice) and only jRCaMP1b in control mice ( $N=2$  mice) while simultaneously recording their behaviour in an open-field arena (Fig. 4a). Because D1-neurons are known to increase their activity during contraversive movements<sup>35,36,38</sup>, we classified neurons that increased firing within 500 ms from the start of contraversive turning movement as turning-related neurons (28 out of 86 recorded neurons from 3 mice, 6–22 trials per mouse). The turning angle was computed after labelling each frame in DeepLabCut<sup>39</sup> (Fig. 4b,c). First, we used DeepLabCut to mark two points, one on the head and one on the back of the mouse, and used these points to generate a ‘head-body’ vector. We compared 2 successive frames (50 frames per second) to calculate the change in vector angle, which was used as a measure of turning. We used the derivative of the head-body vector as a measure of the angular deviation of body posture, regardless of whether the mouse was walking or not. We selected 15 of the turning-related neurons (5 neurons in each mouse) for stimulation (representative mouse shown in Fig. 4d). Selective stimulation of these neurons elicited turning that was comparable to the mice’s natural turning (Fig. 4g,h, in comparison with Fig. 4b,e). Surprisingly, stimulating 5 neurons was sufficient to produce contraversive turning. Different parameters of stimulation can produce contraversive turning (Extended Data Fig. 2b). The magnitude of the behavioural effect depended on the number of neurons stimulated (Extended Data Fig. 2). In contrast, stimulating 5 neighbouring neurons that are not related to turning did not produce significant turning (Fig. 4g,h, D1-cre mice, 25 trials for stimulated neurons, 20 trials for neighbouring neurons; 16 trials in 2 control mice).

We next performed the same experiment with A2A-Cre mice ( $N=3$  jRCaMP1b and ChR2 mice,  $N=2$  controls with only jRCaMP1b) (Fig. 5a). Activation of the indirect pathway neurons is known to produce ipsiversive turning<sup>34</sup>. Out of 354 recorded iSPNs, 36 were related to ipsiversive turning. We selected 12 neurons (4 neurons in the FOV in each mouse) that showed robust excitation

during ipsiversive turning ( $N=3$  mice; Fig. 5b,c). We then excited these turning-related neurons ( $n=12$  neurons from 3 mice), which produced ipsiversive turning (Fig. 5e,g). The magnitude of the turning effect depended on the number of neurons stimulated (Extended Data Fig. 3). Different parameters of stimulation can also produce ipsiversive turning (Extended Data Fig. 4). We also stimulated neurons that were not active during turning, which did not produce significant ipsiversive turning.

Moreover, the effect of selective stimulation was also stable across time. We had selectively stimulated a specific ensemble of neurons on 1 d and replicated the behavioural effect by stimulating the same neurons 40 d later (Extended Data Fig. 5, 2 A2A-cre mice). There was no significant difference in the ipsiversive turning that was elicited on day 1 compared with that on day 40.

**Synthesizing sequences and sweeping patterns of stimulation.** To test the effect of arbitrary stimulation patterns, we used two sequential patterns to activate turning-related neurons: either lateral to medial (LM, starting with the most lateral neuron) or medial to lateral (ML, starting with the most medial neuron) (Fig. 6b,c). Both sequences produced contraversive turning (Fig. 6d).

MAPSI also makes it possible to produce arbitrary spatiotemporal patterns of light to sculpt neural activity. We programmed the DMD to produce rectangular sweeping patterns that covered ~2 % of the FOV. We used two different directions (ML or LM) across the FOV in both hemispheres (Fig. 6f). In D1-Cre mice ( $N=3$ ), either pattern produced contraversive turning, but there was no significant difference between different sweep directions (ML or LM) regardless of hemisphere stimulated (Fig. 6g,h).

We next performed the same experiments using A2A-Cre mice (Fig. 7a). We identified neurons that were active during ipsiversive turning and used the same sequential patterns as used in Fig. 6 (Fig. 7b). We also verified the calcium activity during the sequential pattern stimulation (Fig. 7c). Both sequences produced ipsiversive turning, with the LM sequence (#1) producing greater ipsiversive turning (Fig. 7d). We then used the sweeping patterns used in Fig. 6: ML or LM sweep across the FOV in both hemispheres (Fig. 7f). The rectangular sweep, both ML and LM sweeps, significantly increased ipsiversive turning compared with controls, but there was no significant difference between different sweep directions (ML or LM) (Fig. 7g). If we swept across the FOV over 5 s, both ML and LM sweeping stimulation produced more turning than controls, and LM produced significantly greater turning compared with ML sweeps (Fig. 7h).

## Discussion

The MAPSI system can (1) provide near-cellular resolution stimulation (Figs. 1 and 2), (2) stimulate and record from selected neurons and simultaneously record activity in other neurons in the FOV (Fig. 3), (3) identify neurons active during a specific behaviour and then selectively activate the relevant neuronal ensembles to reproduce the behaviour (Figs. 4 and 5), (4) recreate the recorded spatiotemporal pattern with stimulation and (5) synthesize arbitrary stimulation patterns in the FOV (Figs. 6 and 7).

A major challenge in optogenetics is to control the spatial location and extent of photostimulation. Traditionally, light delivery is achieved with flat-faced optical fibres that illuminate a relatively fixed brain volume around the tip of the fibre. Although recently developed optogenetic methods can control the extent of light delivery, it is difficult to generate patterned stimulation with high resolution in freely behaving mice without using a 2P setup<sup>40</sup>. Although 2P methods can achieve cell-specific stimulation, they require expensive setups and often cannot be performed in freely moving animals. In contrast, MAPSI makes it possible to synthesize complex spatiotemporal sequences of neural activity in any brain region in freely moving animals.

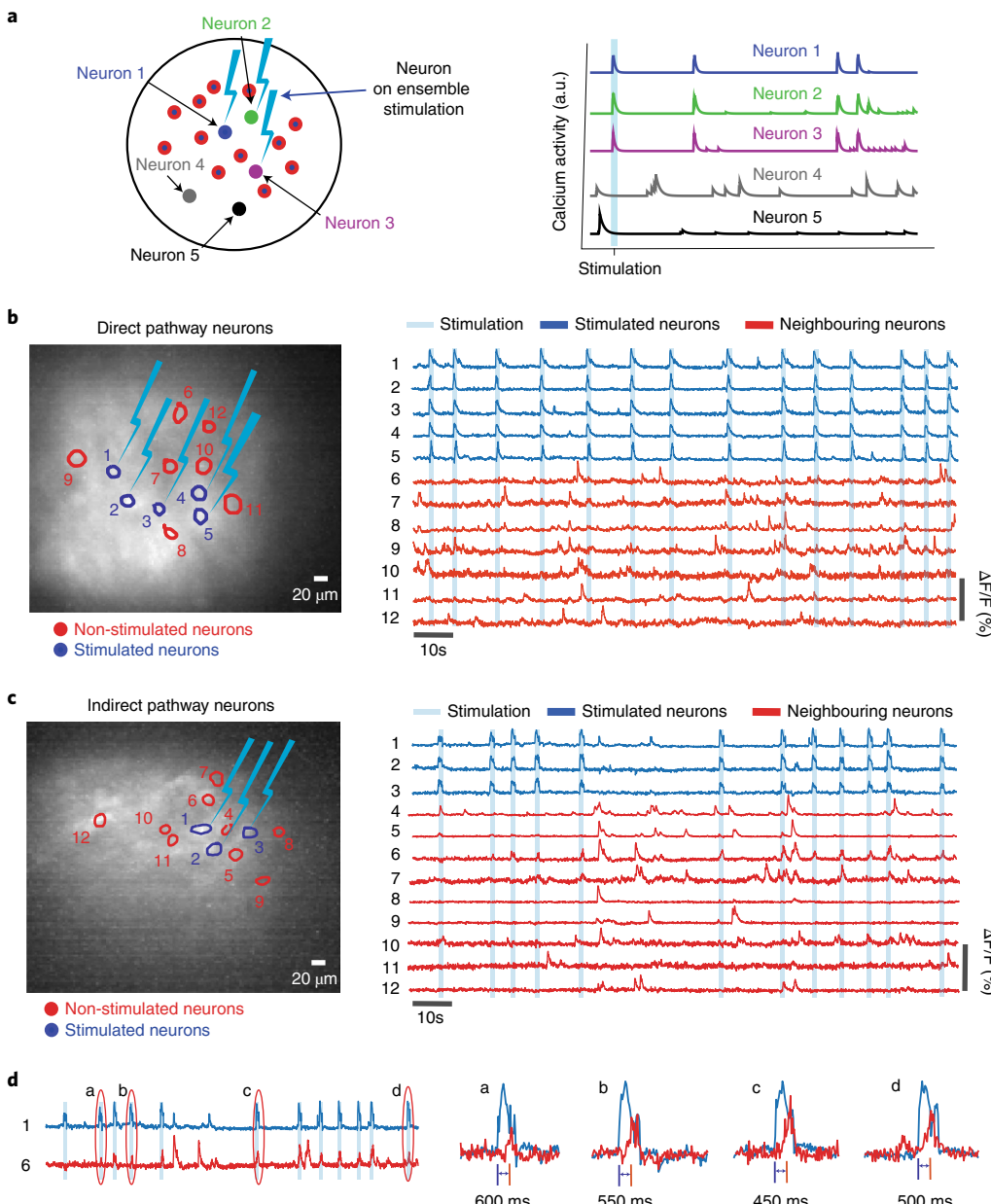


**Fig. 3 | Resolution of MAPSI stimulation in freely behaving animals.** **a**, Left: multiple neurons are selected for simultaneous stimulation. Right: 5 representative traces; the top 3 are directly stimulated neurons and the bottom 2 are neighbouring neurons that were not stimulated. **b**, Calcium signal from dSPNs expressing jRCaMP1b and ChR2. When 5 selected neurons were stimulated, neighbouring neurons were not activated. Left, selected neurons. Right, traces from stimulated neurons and neighboring neurons. **c**, Calcium signal from iSPNs co-expressing jRCaMP1b and ChR2 in a representative mouse. When stimulating 3 neurons, neighbouring neurons were not excited by the stimulation. Left, selected neurons. Right, traces from stimulated neurons and neighboring neurons. **d**, Comparison of neuron 1 and neuron 6 from c. Magnified traces shown on the right. Neuron 1 is directly activated by photostimulation. Although the neighbouring neuron 6 is often activated by the stimulation, the evoked activity is highly variable with a long latency (~500 ms). This pattern suggests that neuron 6 is indirectly activated, presumably via some circuit connection involving multiple synapses.

An important caveat is that single-cell resolution has not been demonstrated in our system since we cannot adjust the stimulation along the  $z$  axis. As described above, a  $10\text{ }\mu\text{m}$  spot on the selected neuron could potentially penetrate up to  $30\text{ }\mu\text{m}$  below the surface of the GRIN lens. Given the size of SPNs ( $\sim 12\text{--}15\text{ }\mu\text{m}$  diameter), it is possible that additional neurons located just beneath the selected neurons were also activated. However, even in this scenario, we do not expect many neurons to be affected. Depending on the size of the neuron and the density in the brain area in question, MAPSI can approach cellular resolution in many instances. Since opsins

expression may not be confined to the soma, it is possible that the processes of some opsin-expressing neurons nearby might be excited as well, but this possibility could be minimized by using soma-targeted opsins<sup>41</sup>.

Using a DMD, we were able to generate precise beamlets that can target single or multiple user-selected neurons with single-cell resolution. We tested this design in freely moving mice by simultaneously recording and stimulating direct and indirect pathway neurons *in vivo*. We were able to replay the recorded calcium activity in a small group of neurons and reproduce the same behaviour

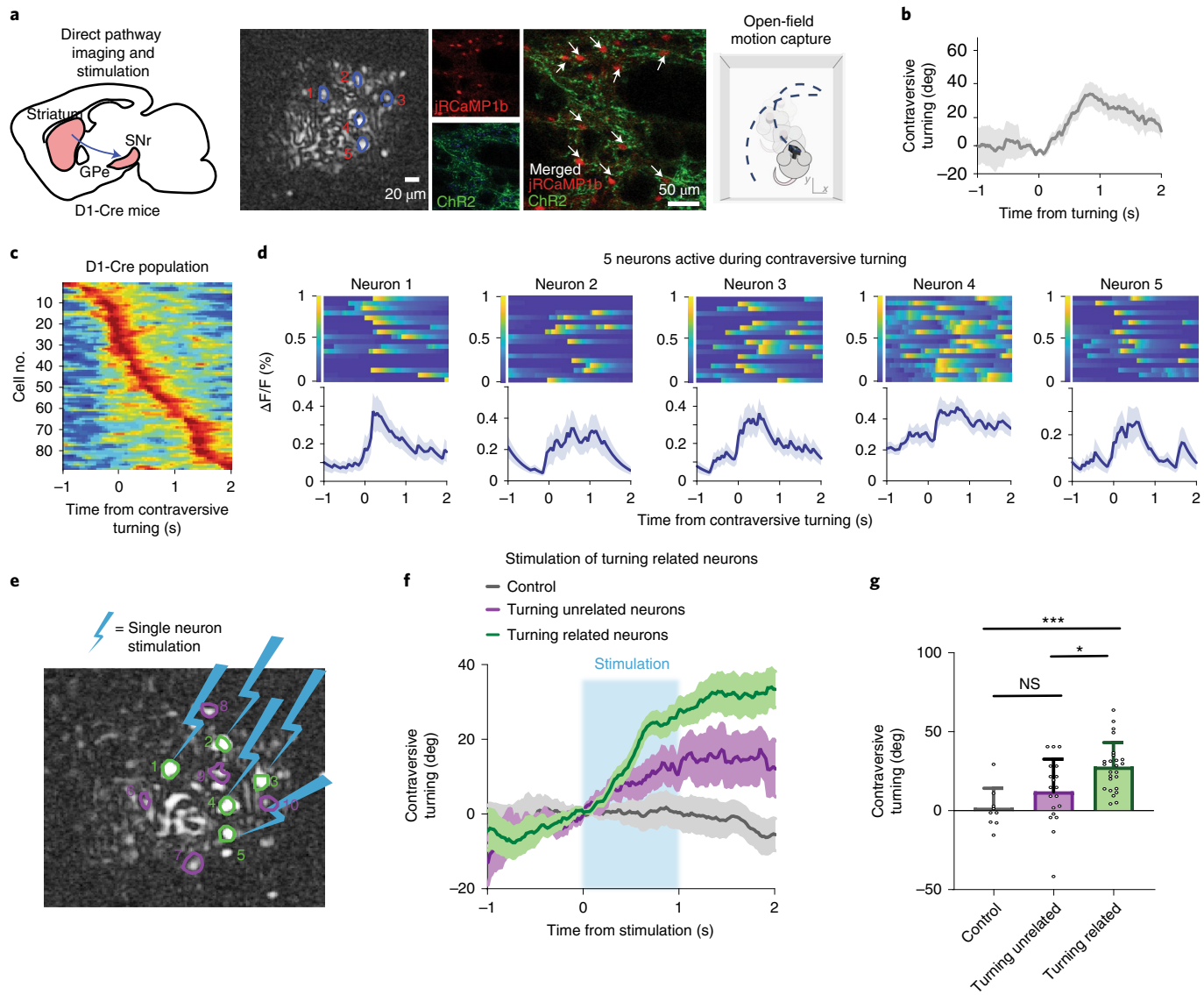


**Fig. 4 | Stimulation of direct pathway neurons that are active during contraversive turning reproduces contraversive turning.** **a**, Left, drawing of the direct pathway in the basal ganglia. Middle, 5 selected D1+ dSPNs from a representative mouse in an open-field arena were stimulated. These neurons co-express ChR2 and jRCaMP1b. Right, turning behavior in a mouse, as quantified by motion capture. Dashed lines indicate possible trajectory. **b**, Behavioural data were aligned to the start of contraversive turning (3 D1-cre mice, 6–22 trials per mouse). **c**, All recorded dSPNs (3 D1-cre mice, 86 neurons) aligned to contraversive turning and sorted according to turning onset. **d**, Calcium activity of 5 neurons in a representative mouse, activated during contraversive turning onset. **e**, The same 5 neurons were stimulated, while 5 neighbouring neurons not related to turning were also stimulated. **f**, Stimulating 5 selected neurons produced more contraversive turning than stimulating unrelated neurons or stimulation in control mice (3 D1-cre mice, 5–25 trials of stimulated neurons, 4–20 trials per mouse; 2 control mice, 6–16 trials per mouse). **g**, Stimulation of 5 turning-related neurons significantly increased contraversive turning angle compared with controls and unrelated neurons stimulation (one-way analysis of variance (ANOVA): Stim groups,  $F_{(2,50)} = 9.303$   $P = 0.0004$ ). Tukey's post hoc analysis revealed that stimulating contraversive turning-related neurons resulted in more turning than stimulating neighbouring neurons ( $*P = 0.0120$ ) and controls ( $***P = 0.0007$ )). Stimulating unrelated neurons did not produce more turning than controls ( $P = 0.2819$ ; NS, not significant). All error bars (including shaded regions) indicate s.e.m.

(Figs. 6 and 7). This is a demonstration that selective stimulation of a few SPNs could result in turning behaviours. In either direct or indirect pathways, activation of as few as 3 SPNs could produce significant turning, contraversive for dSPNs and ipsiversive for iSPNs. The amount of turning depends on the number of turning-related neurons activated and activation of 5 neurons produced a comparable amount of turning as stimulation of the entire FOV (Extended Data Figs. 2 and 3). This is not surprising since in the FOV the number of SPNs that are specifically related to turning is low and stimulating the whole field would additionally activate

neurons with presumably other functions. These results suggest that the number of SPNs involved in generating a specific action is much lower than expected.

Current systems that are capable of patterned stimulation and imaging usually require large microscopes and are difficult to use in freely moving animals<sup>13,42</sup>. The best example of a 1P system that can be used in freely moving animals is a fiberscope system developed by Szabo and colleagues<sup>22</sup>, but their system has several limitations. First, it requires a confocal microscope as well as two separate lasers, whereas our system does not. Secondly, with the fiberscope system,

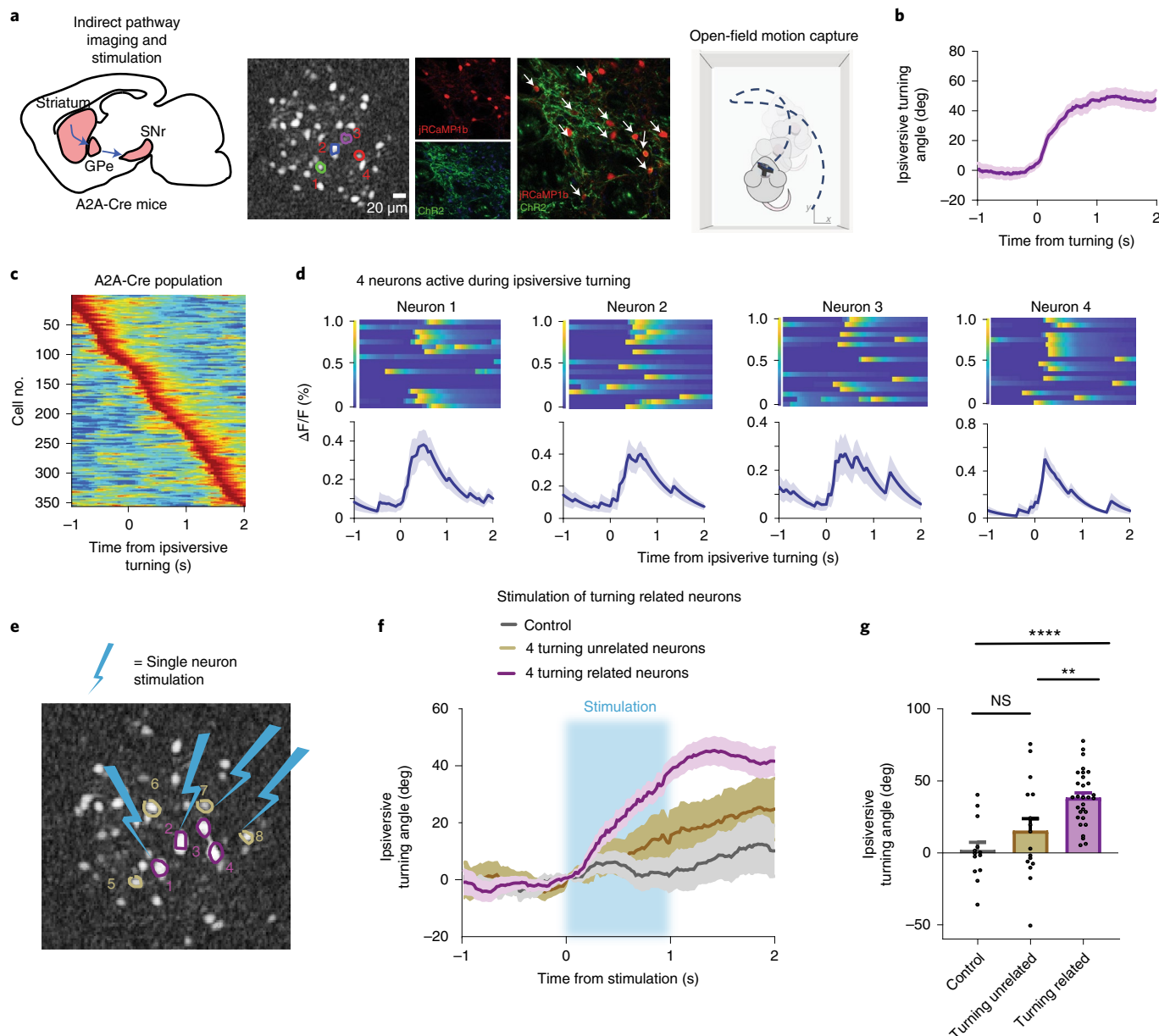


**Fig. 5 | Selective stimulation of indirect pathway neurons that are active during ipsiversive turning recapitulates ipsiversive turning.** **a**, Left, drawing of the direct pathway in the basal ganglia. Middle, 4 selected A2A+ DLS neurons from a representative mouse in an open-field arena were stimulated. Neurons co-expressing both ChR2 and jRCaMP1b are shown. Right, turning behavior in a mouse, as quantified by motion capture. Dashed lines indicate possible trajectory. **b**, Behavioural data were aligned to the onset of ipsiversive turning relative to the hemisphere being recorded from 3 A2A-cre mice (5–28 trials per mouse). **c**, All recorded A2A+ neurons (3 A2A-cre mice, total of 354 neurons, >50 neurons per mouse) aligned to ipsiversive turning and sorted according to turning onset. **d**, Four neurons were selected from a representative mouse, activated during ipsiversive turning. Data were aligned to ipsiversive turning onset. **e**, The same 4 neurons from one sample mouse were stimulated. Four neighbouring neurons that were not highly related with turning were also stimulated. **f**, Optogenetic excitation of the 4 selected neurons produced significantly more ipsiversive turning compared with controls (no opsin expression) or unrelated neurons (3 A2A-cre mice, 6–30 trials per mouse for stimulated neurons, 3–16 trials per mouse for unrelated neurons; 2 control mice, 6–13 trials per mouse). **g**, Stimulation increased ipsiversive turning (one-way ANOVA: Stim,  $F_{(2,56)} = 11, P < 0.0001$ ). Tukey's post hoc analysis revealed that stimulation of turning-related neurons produced greater ipsiversive turning compared with stimulation of unrelated neurons (\*\* $P = 0.0096$ ) or of controls (\*\*\*\* $P < 0.0001$ ), but stimulating unrelated neurons did not produce more ipsiversive turning than controls ( $P = 0.2932$ ). All error bars (including shaded regions) indicate s.e.m. See also Supplementary Video 2.

lateral and axial resolution can be degraded when the animal is moving with the optic fibre. More importantly, in their system the wavelength for ChR2 stimulation overlaps with the excitation wavelength of the calcium indicator (GCaMP5), so some neurons could be excited during calcium imaging. The FOV for stimulation and recording using their fiberscope system is also limited by the

properties of the coupled micro-objective. There is also a commercially available 1P fiberscope (<https://www.mightexbio.com/products/oasis/oasis-implant/>). This system has the advantage of a large FOV (0.5–3.2 mm) and a small implant (0.7 g), but has similar limitations as just described. On the other hand, our system uses a GRIN lens, which makes it possible to move the baseplate to move

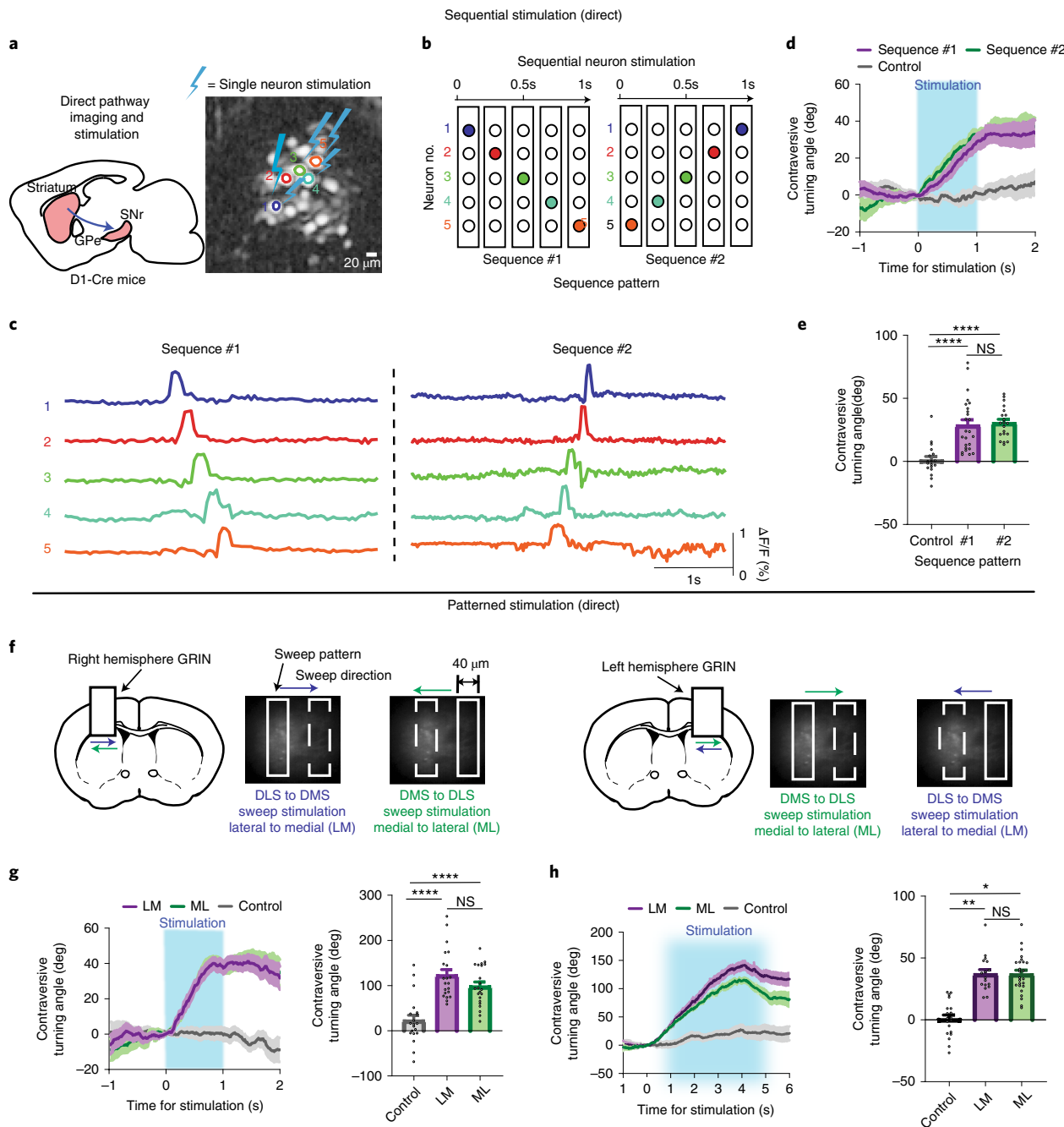


**Fig. 6 | Sequential and patterned stimulation of the direct pathway causes contraversive turning.** **a**, D1-Cre mice were used with MAPSI for single-neuron sequence stimulation from a representative mouse. Left, drawing of the direct pathway. Right, neurons selected for stimulation. **b**, Five neurons were stimulated in two different sequences. The schematic shows the order and sequence of neurons that were stimulated. The two sequences either progressed laterally-to-medially (sequence #1) or medially-to-laterally (sequence #2). See also Supplementary Video 3. **c**, Calcium traces for the selected neurons from each sequence, showing the time course of their activation. **d**, single neuron activity evoked by stimulation patterns. **e**, summary of turning behavior produced by stimulation. Stimulation of the 5 neurons in both sequences greatly increased maximum contraversive turning compared with controls, but there was no difference in the direction of the sequence (one-way ANOVA,  $F_{(2,60)} = 4.112$ ,  $P < 0.0001$ ). Tukey's post hoc analysis revealed that both sequences produced significantly more contraversive turning than controls ( $****P < 0.0001$ ,  $****P < 0.0001$ ), but were not different from each other ( $P = 0.9277$ ) (3 D1-Cre mice, 5–25 trials for #1, 4–20 trials for #2, 2 control mice, 6–18 trials per mouse)). **f**, Schematic of sweeping stimulation experiment where a 20- $\mu$ m-wide bar moved horizontally from lateral side to medial side (LM) or from medial side to lateral side (ML). **g**, Left: sweeping stimulation for 1 s increased contraversive turning compared with controls. Right: there was a significant main effect of stimulation vs non-stimulation (one-way ANOVA  $F_{(2,58)} = 0.1825$ ,  $P = 0.8336$ ). Tukey's post hoc analysis revealed that comparison of sequences LM vs ML was not significant ( $P = 0.9996$ ) but LM vs controls ( $****P < 0.0001$ ) and ML vs controls ( $****P < 0.0001$ ) were significant; 3 D1-Cre, 4–17 trials LM, 6–25 trials for ML; 2 controls, 5–19 trials per mouse). **h**, Sweeping stimulation for 5 s significantly increased contraversive turning compared with controls. There was a main effect of stimulation ( $F_{(2,12)} = 5.88$ ,  $P = 0.017$ ). Tukey's post hoc analysis, however, revealed no significant difference between sequence #1 and #2 ( $P = 0.74$ ), but a significant difference between sequence #1 and controls ( $**P = 0.0023$ ) and between sequence #2 and controls ( $*P = 0.049$ ) (3 D1-Cre mice, LM: 5–21 trials per mouse, ML: 5–25 trials per mouse; 3 controls, LM and ML, 6–20 trials per mouse). All error bars (including shaded regions) indicate s.e.m.

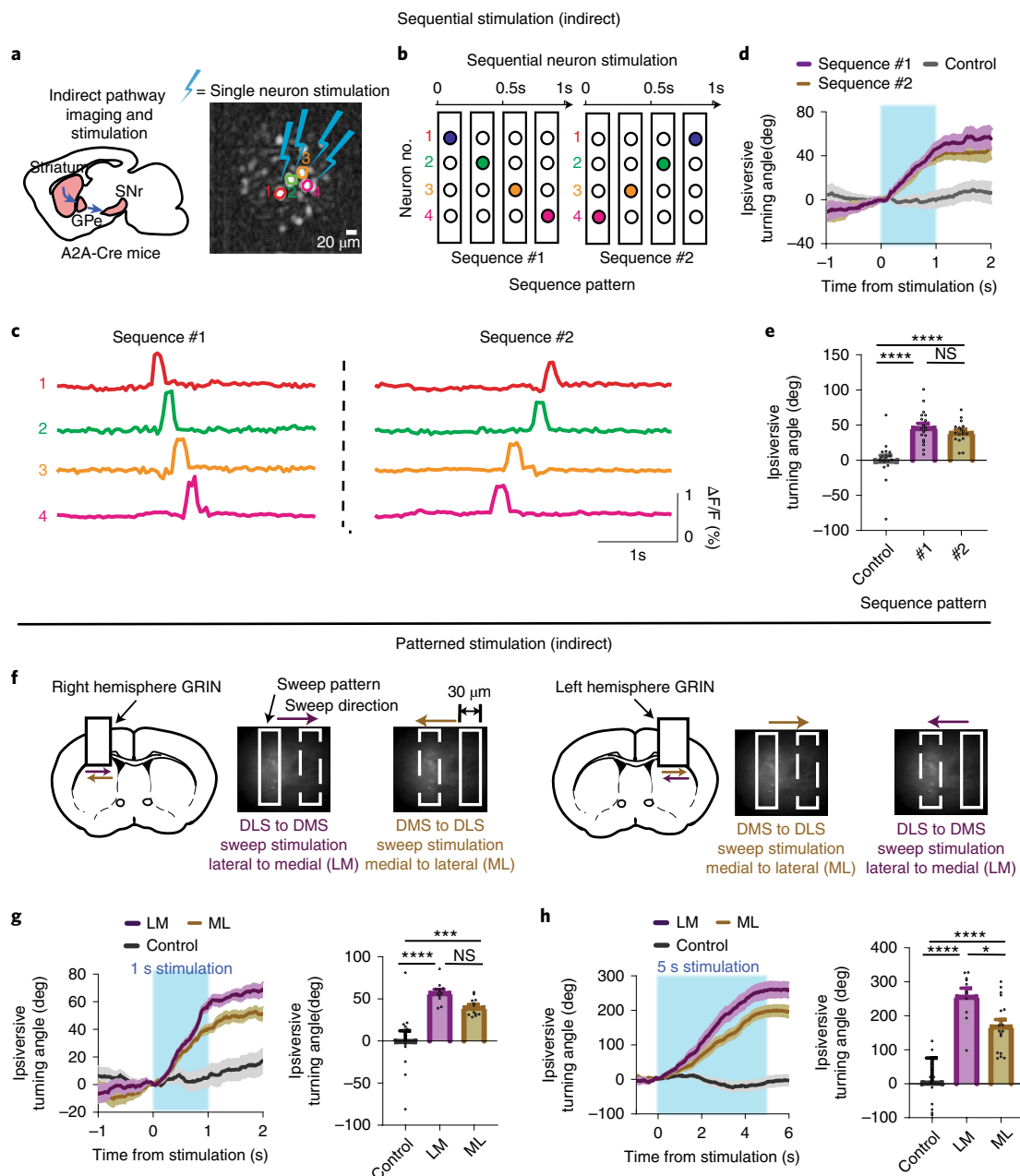


**Fig. 7 | Sequential and patterned stimulation of the indirect pathway causes ipsiversive turning.** **a**, A2A-Cre mice were used with MAPSI for single-neuron sequence stimulation. Left, drawing of the direct pathway. Right, neurons selected for stimulation. **b**, Four neurons were optogenetically excited in two different sequences. The schematic shows the order and sequence of neurons that were stimulated. Rows indicate individual neurons and columns indicate individual time points. The two sequences either progressed laterally-to-medially (sequence #1) or medially-to-laterally (sequence #2). **c**, Calcium traces for the 4 selected neurons from each sequence, showing the time course of their activation. **d**, Single neuron activity evoked by stimulation patterns. **e**, Summary of turning behavior produced by stimulation. Stimulation of the 4 neurons in both sequences significantly increased ipsiversive turning compared with controls (one-way ANOVA,  $F_{(2,5)} = 0.63$ ,  $P = 0.5367$ ; #1 vs #2:  $P = 0.6191$ ; #1 vs control: \*\*\*\* $P < 0.0001$ ; #2 vs control: \*\*\*\* $P < 0.0001$ ; 3 A2A-cre mice, 3–19 trials of LM per mouse, 3–17 trials of ML per mouse; 2 controls, 6–18 trials per mouse). **f**, Schematic of sweeping stimulation experiment. A 20- $\mu$ m-wide bar moved horizontally from lateral side to medial side (LM) or from medial side to lateral side (ML). See also Supplementary Video 4. **g**, Sweeping stimulation for 1 s significantly increased ipsiversive turning compared with controls. Sweeping from lateral to medial also produced more ipsiversive turning. Ipsiversive turning was significantly higher than controls for both sequences, but was not significantly different between sequences (one-way ANOVA,  $F_{(2,12)} = 14.79$ ,  $P = 0.0006$ ). Tukey's post hoc analysis revealed that sequence #1 was not significantly different from sequence #2 ( $P = 0.24$ ), but sequence 1 (\*\*\*\* $P = 0.0005$ ) and sequence 2 (\*\* $P = 0.0092$ ) were significantly greater than controls (3 A2A-cre mice, 4–12 trials of LM per mouse, 3–12 trials of ML per mouse; 2 controls, 4–12 trials per mouse). **h**, Sweeping stimulation for 5 s significantly increased ipsiversive turning compared with controls, and the LM sweep produced more ipsiversive turning compared with the ML sweep (one-way ANOVA,  $F_{(2,12)} = 47.68$ ,  $P < 0.0001$ , 3 A2A-cre mice, 3–10 trials per mouse for LM and 4–17 trials for ML; 2 control mice, 6–13 trials per mouse). Tukey's post hoc analysis revealed that both sequences produced more ipsiversive turning than the control (\*\*\*\* $P < 0.0001$  for both), LM vs ML: \* $P = 0.0132$ . All error bars (including shaded regions) indicate s.e.m.

the FOV to a different region covered by the lens. Thus, many neurons can be recorded and stimulated from a single animal.

In MAPSI, because the dual-beam paths are independent of each other, neurons selected for stimulation can be simultaneously recorded along with the activity of other neurons in the FOV. It therefore allows both manipulation and recording of any recorded neuron at the same time in freely moving animals. As such, MAPSI can be used to interrogate neuronal circuit function and investigate mouse models of neurological and psychiatric disorders. For example, it would be useful to characterize pathological neural activity in disease models to determine whether they play a causal role in the key symptoms, and also to rescue function by artificially introducing more normal patterns of neural activity. In short, given its portability and low cost, MAPSI provides a powerful tool for understanding the neural basis of behaviour.

## Methods

**Experimental animals.** All experimental procedures were approved by the Animal Care and Use Committee at Duke University. Male D1-Cre mice (Jackson Labs, Drd<sup>1tm2.1StJ</sup>) and A2A-Cre mice (Adora2A<sup>tm1Dgj/J</sup>) were used. All mice were between 3–8 months old, group housed and maintained on a 12:12 h light cycle. Testing was always performed during the light phase.

**Viruses.** pAAV.CAG.Flex.NES-jRCaMP1b.WPRE.SV40 was a gift from Douglas Kim and the GENIE Project (Addgene viral prep 100849; <http://n2t.net/addgene:100849>; RRID: Addgene 100849). pAAV-EF1a-double floxed-hChR2(H134R)-EYFP-WPRE-HGHpA was a gift from Karl Deisseroth (Addgene plasmid 20298; <http://n2t.net/addgene:20298>; RRID: Addgene\_20298).

**Surgery and histology.** Mice were initially anaesthetized with 5.0% isoflurane and maintained at 1–2% during surgery. A craniotomy was made to allow implantation of the GRIN lens (Bregma +0.0–1.0 mm AP, ±2.0–2.7 ML). Pulled pipettes were used to inject the virus using a Nanoject III injector (Drummond Scientific). The first virus injection (250 nl of pAAV.CAG.Flex.NES-jRCaMP1b.WPRE.SV40) was injected at two sites (+0.25, +0.75 AP, 2.5 ML), each with 5 depths (2.8–2.0 dorsal-ventral (DV)). Injections were made at a rate of 1 nl s<sup>-1</sup>. The second injection (250 nl of AAV(9)-EF1a-DIO-hChR2(H134R)-EYFP) was then injected at the same coordinates. The injection pipette was always left in place for 3 min after each injection to allow for maximum absorption before it was retracted.

After the virus injection, aspiration was performed from the brain surface and a GRIN lens (1.8 mm × 4.3 mm, Edmund Optics) was implanted in the DLS above the injection site. The lens was secured to the skull using dental cement and covered with Kwik-Sil to protect the lens surface. At 5–6 weeks after the GRIN lens implantation, baseplating was performed under visual guidance of the calcium signal to determine the best FOV.

After the completion of experiments, mice were transcardially perfused with 0.1 M phosphate buffered saline (PBS), followed by 4% paraformaldehyde to confirm placement and viral expression. The brains were then transferred to a 30% sucrose solution and sliced coronally using a cryostat (Leica CM1850). Slices were mounted with DAPI-mounting medium (Vector Laboratories, Vectashield, H-1800) to identify the nuclei of neurons. Slices were then imaged using an inverted confocal microscope (Zeiss LSM780 and LSM880) for zoomed-in images, or an upright epifluorescence microscope for whole brain images (Axio Imager.M1, Zeiss).

**Filters and LED control.** A LUXEON Rebel Colour lime LED (LXML-PX02-0000) filtered with a 540–580 nm excitation LED filter (Chroma ET560/40x) was used for calcium imaging, while a 473 nm blue laser filtered with a 450–490 nm excitation laser filter (Chroma ET470/40x) was used for optogenetic stimulation. The two colours are combined through the excitation dichroic mirror (Chroma 59003bs) by merging them in the excitation light path. The main dichroic mirror (Chroma 69013bs) reflects the excitation light into the GRIN lens, while the fluorescence image passes through the emission filter. The emission filter (Chroma ET630/75) is designed to avoid crosstalk from the excitation light. In addition, an absorber (Chroma ET775/50x) was located beneath the DMD to avoid reflected blue light during the off-state that could potentially scatter into the excitation light path (Supplementary Fig. 2).

The output from the lime LED is controlled by a current supply combined with two parallel chips (LT3092ETS8), which supply 2.9 V of voltage and enough current to power the LED. The constant current source can provide up to 200 mA of current (up to 12 mW mm<sup>-2</sup> measured beneath the GRIN lens) with a step size of 4 mA. A programmable potentiometer (MCP4018) is used to adjust the current using control signals from an Arduino UNO (Arduino), which communicates with the computer. Custom scripts are used to adjust the parameters of calcium imaging.

**DMD design and installation.** For patterned stimulation, we used a DMD (Texas Instruments, DLP2010), which is a digitally controlled micro-opto-electromechanical system that modulates spatial light to generate

different light stimulation patterns. This DMD has on its surface more than 400,000 microscopic mirrors arranged in a rectangular array, with a resolution ratio of 854 × 480 pixels. Each mirror has a hinge and hook beneath it, allowing it to rotate ±17° (relative to the flat surface) to switch between on and off-states. The ‘on-state’ is defined by each of the mirrors’ positions corresponding to the tilt angle  $\theta$  (+17°) such that the reflected light is directed towards the excitation light path. When a mirror is positioned in the opposite direction, the mirror is in the ‘off-state’. In this state, light is reflected into the absorber rather than into the GRIN lens, preventing light leak in the specified FOV (Supplementary Fig. 2). To ensure that in the off-state, all the light will be reflected to the absorber without any light scattering, the DMD rotation angle must be limited as follows:

$$\begin{cases} 2(\alpha + \theta) < 90^\circ \\ \alpha + 3\theta < 90^\circ \end{cases} \quad (1)$$

where  $\theta$  is the DMD rotation angle and  $\alpha$  is the mirror tilt angle. We set  $\alpha = 13^\circ$  as the optimal rotation angle.

**Miniscope housing design and simulation in software.** The miniscope body size is small, while the distance between the laser source and the GRIN lens is 20 mm. To ensure that we can generate precise patterns beneath the GRIN lens and to have sufficient energy for excitation, the beam divergence for the laser light must be less than 4° (Supplementary Fig. 3). The collimation deviation is calculated by the following equation:

$$\eta = \frac{R_{D1} - R_{D50}}{R_{D1}} \quad (2)$$

where  $R_{D1}$  is the radius of the illumination field when the target screen is 1 mm from the outer surface of the collimation lens,  $R_{D50}$  is the radius of the illumination field when the target screen is 50 mm from the surface and  $\eta$  is the collimation deviation. The smaller the deviation, the more precisely collimated the light is.

After the placement and operation of all the filters and lenses were confirmed, a 3D model housing all the components was designed in Solidworks software. To verify the optic simulation designs, we imported all the 3D models into the software programme Tracepro (Supplementary Fig. 2). The miniscope body was then printed using a 3D printer (Multi-Jet Fusion technology) with Nylon PA12.

**Miniscope control system design.** MAPSI is based on the original UCLA open source Miniscope<sup>23</sup>. It includes a CMOS imaging sensor, a PCB board, all the optical components such as the emission and excitation filters, GRIN lens, achromatic lens and data acquisition system (DAQ) hardware and software. The image sensor resolution is 752 px × 480 px and the frame rate is up to 60 Hz. However, the original Miniscope design was significantly modified to allow separate light paths.

MAPSI contains an LED power source, a recording subsystem and a pattern control subsystem (Supplementary Fig. 1). Two computers are needed: one that connects with all the subsystems to send and receive data as well as to send commands, and a second computer to project the photostimulation patterns into the pattern control subsystem. The first computer runs two programmes: the original miniscope recording software and the integration software application that controls the LED power subsystem, which sends synchronous commands to all the other subsystems to ensure timestamps are all aligned. An Arduino UNO that is connected with this computer sends and receives the synchronous commands from/to the CMOS to control the LED current and the pattern. A National Instruments box is also connected with this computer and sends TTL signals to control the laser generator (RL639T8-500).

The DMD is controlled by a custom-designed driver board with a 60 cm enamelled wire cable. One computer sends image data to the HDMI interface using a wireless HDMI kit (Diamond VS75). The pattern control subsystem receives the pattern image data from the computer and controls the DMD (Texas Instruments; DLPC3430 and DLPA2000). An HDMI data interface board transmits signals from the computer to the DLPC3430.

**Determining z-axis resolution of MAPSI.** The MAPSI z-axis resolution was determined in brain slices placed on a confocal microscope (Zeiss, LSM880) equipped with a 20x objective (numerical aperture = 0.8). Using a vibratome, we cut 200 µm coronal sections from a mouse brain co-expressing RCaMP1b and ChR2. The slice was adhered to the bottom of a culture dish and the GRIN lens was placed just above the slice. The GRIN lens and the tissue were then embedded together with 4% agarose gel. MAPSI was then fixed on the top of the GRIN lens and attached to a stereotaxic frame to obtain a good focal pattern image (Fig. 2b). A confocal microscope was used to image the slice from the bottom of the dish while simultaneously using MAPSI to target single neurons from the top of the dish. While MAPSI was generating a pattern on the tissue, RCaMP1b images were acquired using a 561 nm excitation laser and 2 detectors (photo-multiplier tube for the pattern and Gallium Arsenide Phosphide detector for RCaMP) (pixel size, 0.21 µm × 0.21 µm × 0.70 µm; pinhole size, 1 airy unit). The total energy detected beneath the GRIN lens was measured using an optical power metre (PM100A).

**Calibration of MAPSI.** To match DMD and CMOS pixel location, we used a 60 µm brain slice co-expressing jRCaMP1b and ChR2. GRIN lens was placed on the brain slice and MAPSI was fixed on the top of GRIN lens. Once an image with white spot (diameter, 10 pixels) and black background was projected on DMD, a spot fluorescence image was recorded on CMOS (Supplementary Fig. 2g). As the white spot was moved in one axis, the movement of the fluorescence spot was also captured. Based on the DMD pixels (854 × 480) and the CMOS pixels (752 × 480), we were able to calibrate the white spot position and fluorescence spot position with the linear relationship:

$$\frac{5P_{\text{DMD}-X}}{7} + 166 = P_{\text{CMOS}-X} \quad (3)$$

where  $P_{\text{DMD}-X}$  is the  $x$ -axis position on DMD and  $P_{\text{CMOS}-X}$  is the  $x$ -axis pixel position on CMOS.

$$\frac{10P_{\text{DMD}-Y}}{11} + 13 = P_{\text{CMOS}-Y} \quad (4)$$

where  $P_{\text{DMD}-Y}$  is the  $y$ -axis position on DMD and  $P_{\text{CMOS}-Y}$  is the  $y$ -axis pixel position on CMOS.

Once a neuron was identified for stimulation, the pixels' location of that neuron could be imported into equations (3) and (4) to calculate the matching pixels' location on DMD. The projection image was then created with the calculated pixels.

**Open-field behaviour recording and analysis.** Mice were tested in an open-field arena (25 cm × 25 cm). A high-speed camera (FLIR BFS-U3-04S2M) was placed above the platform to record the behaviour of the mice at 50 frames per second. The DMD driver and HDMI interface board were fixed on the tuning holder, connected to the DMD using a 60 cm enamelled wire cable which prevents tangling of the wires and allows the mice to move freely. Other wires (coaxial cable for CMOS, power wire for LED) pass through the centre hole of the ball bearing (Extended Data Fig. 1a).

Behavioural data recorded by the cameras were analysed using DeepLabCut<sup>39,43,44</sup>. Three markers (head, body and tail) were labelled in each video. Samples (200) of frames were auto selected from each video and 18 videos were taken for training with the 200,000 training iterations. The test error was 4.37 pixels and the training error was 1.63 pixels. The resulting data were then imported into MATLAB where behavioural variables, such as displacement and turning angle, were created using a custom script. The processed data were then imported into Neuroexplorer 5 along with the calcium imaging data for further analysis.

**Statistical analyses.** All statistical analyses were performed in GraphPad Prism 7.0. All error bars represent s.e.m. Significance levels were set to  $P < 0.05$ . Significance for comparisons: \* $P < 0.05$ , \*\* $P < 0.01$ , \*\*\* $P < 0.001$ , \*\*\*\* $P < 0.0001$ .

**Calcium imaging acquisition and analysis.** A CMOS imaging sensor, a DAQ and a USB host controller were used for calcium imaging. Images were acquired at 20 frames per second and recorded to uncompressed '.avi' files using the DAQ software. The videos were then imported into MATLAB for non-rigid motion correction<sup>44</sup>, followed by deconvolution with the constrained non-negative matrix factorization algorithm<sup>45</sup>. Seed pixels were initialized with a minimum local correlation value of 0.8 and a minimum peak-to-noise ratio of 10. The minimum number of non-zero pixels for each neuron was set at 10 on the basis of the resolution of the CMOS sensor (1 µm per pixel). Both deconvolved and raw calcium traces were saved.

**Ethical compliance.** All research reported in this study was approved by the Duke University Institutional Animal Care and Use Committee (protocol A254-19-11).

**Reporting summary.** Further information on research design is available in the Nature Research Reporting Summary linked to this article.

## Data availability

The main data supporting the results in this study are available within the paper and its Supplementary Information. The raw and analysed datasets generated during the study are too large to be publicly shared, yet they are available for research purposes from the corresponding author on reasonable request.

## Code availability

The Matlab codes are available from the corresponding author on request.

Received: 9 September 2021; Accepted: 4 July 2022;

Published online: 15 August 2022

## References

- Dana, H. et al. High-performance GFP-based calcium indicators for imaging activity in neuronal populations and microcompartments. *Nat. Methods* **16**, 649–657 (2019).
- Boyden, E. S., Zhang, F., Bamberg, E., Nagel, G. & Deisseroth, K. Millisecond-timescale, genetically targeted optical control of neural activity. *Nat. Neurosci.* **8**, 1263–1268 (2005).
- Yizhar, O., Fenno, L. E., Davidson, T. J., Mogri, M. & Deisseroth, K. Optogenetics in neural systems. *Neuron* **71**, 9–34 (2011).
- Dana, H. et al. High-performance calcium sensors for imaging activity in neuronal populations and microcompartments. *Nat. Methods* **16**, 649–657 (2019).
- Ghosh, K. K. et al. Miniaturized integration of a fluorescence microscope. *Nat. Methods* **8**, 871–878 (2011).
- Kerr, J. N. & Denk, W. Imaging *in vivo*: watching the brain in action. *Nat. Rev. Neurosci.* **9**, 195–205 (2008).
- Hughes, R. N. et al. Precise coordination of three-dimensional rotational kinematics by ventral tegmental area gabaergic neurons. *Curr. Biol.* **29**, 3244–3255. e4 (2019).
- Emiliani, V., Cohen, A. E., Deisseroth, K. & Häusser, M. All-optical interrogation of neural circuits. *J. Neurosci.* **35**, 13917–13926 (2015).
- Zhang, Z., Russell, L. E., Packer, A. M., Gauld, O. M. & Häusser, M. Closed-loop all-optical interrogation of neural circuits *in vivo*. *Nat. Methods* **15**, 1037–1040 (2018).
- Nikolenko, V. et al. SLM microscopy: scanless two-photon imaging and photostimulation using spatial light modulators. *Front. Neural Circuits* **2**, 5 (2008).
- Stamatakis, A. M. et al. Simultaneous optogenetics and cellular resolution calcium imaging during active behavior using a miniaturized microscope. *Front. Neurosci.* **12**, 496 (2018).
- Packer, A. M., Russell, L. E., Dalgleish, H. W. & Häusser, M. Simultaneous all-optical manipulation and recording of neural circuit activity with cellular resolution *in vivo*. *Nat. Methods* **12**, 140–146 (2015).
- Carrillo-Reid, L., Han, S., Yang, W., Akrouh, A. & Yuste, R. Controlling visually guided behavior by holographic recalling of cortical ensembles. *Cell* **178**, 447–457. e5 (2019).
- Rickgauer, J. P., Deisseroth, K. & Tank, D. W. Simultaneous cellular-resolution optical perturbation and imaging of place cell firing fields. *Nat. Neurosci.* **17**, 1816–1824 (2014).
- Yang, W., Carrillo-Reid, L., Bando, Y., Peterka, D. S. & Yuste, R. Simultaneous two-photon imaging and two-photon optogenetics of cortical circuits in three dimensions. *eLife* **7**, e32671 (2018).
- Carrillo-Reid, L., Yang, W., Kang Miller, J.-E., Peterka, D. S. & Yuste, R. Imaging and optically manipulating neuronal ensembles. *Annu. Rev. Biophys.* **46**, 271–293 (2017).
- Wallace, D. J. & Kerr, J. N. Circuit interrogation in freely moving animals. *Nat. Methods* **16**, 9–11 (2019).
- Zong, W. et al. Miniature two-photon microscopy for enlarged field-of-view, multi-plane and long-term brain imaging. *Nat. Methods* **18**, 46–49 (2021).
- Warp, E. et al. Emergence of patterned activity in the developing zebrafish spinal cord. *Curr. Biol.* **22**, 93–102 (2012).
- Zhu, P., Fajardo, O., Shum, J., Schärer, Y.-P. Z. & Friedrich, R. W. High-resolution optical control of spatiotemporal neuronal activity patterns in zebrafish using a digital micromirror device. *Nat. Protoc.* **7**, 1410–1425 (2012).
- Guo, Z. V., Hart, A. C. & Ramanathan, S. Optical interrogation of neural circuits in *Caenorhabditis elegans*. *Nat. Methods* **6**, 891–896 (2009).
- Szabo, V., Ventalon, C., De Sars, V., Bradley, J. & Emiliani, V. Spatially selective holographic photoactivation and functional fluorescence imaging in freely behaving mice with a fiberscope. *Neuron* **84**, 1157–1169 (2014).
- Cai, D. J. et al. A shared neural ensemble links distinct contextual memories encoded close in time. *Nature* **534**, 115–118 (2016).
- Burton, R. A. et al. Optical control of excitation waves in cardiac tissue. *Nat. Photonics* **9**, 813–816 (2015).
- Jung, H., Kang, H. & Nam, Y. Digital micromirror based near-infrared illumination system for plasmonic photothermal neuromodulation. *Biomed. Opt. Express* **8**, 2866–2878 (2017).
- Ren, M., Chen, J., Chen, D. & Chen, S.-C. Aberration-free 3D imaging via DMD-based two-photon microscopy and sensorless adaptive optics. *Opt. Lett.* **45**, 2656–2659 (2020).
- Akerboom, J. et al. Genetically encoded calcium indicators for multi-colour neural activity imaging and combination with optogenetics. *Front. Mol. Neurosci.* **6**, 2 (2013).
- Dana, H. et al. Sensitive red protein calcium indicators for imaging neural activity. *eLife* **5**, e12727 (2016).
- Shemesh, O. A. et al. Temporally precise single-cell-resolution optogenetics. *Nat. Neurosci.* **20**, 1796–1806 (2017).
- Owen, S. F., Liu, M. H. & Kreitzer, A. C. Thermal constraints on *in vivo* optogenetic manipulations. *Nat. Neurosci.* **22**, 1061–1065 (2019).
- Gerfen, C. R., Paletzki, R. & Heintz, N. GENSAT BAC cre-recombinase driver lines to study the functional organization of cerebral cortical and basal ganglia circuits. *Neuron* **80**, 1368–1383 (2013).
- Yin, H. H. The basal ganglia in action. *Neuroscientist* **23**, 299–313 (2017).

33. Mink, J. W. The basal ganglia: focused selection and inhibition of competing motor programs. *Prog. Neurobiol.* **50**, 381–425 (1996).
34. Kravitz, A. V. et al. Regulation of Parkinsonian motor behaviours by optogenetic control of basal ganglia circuitry. *Nature* **466**, 622–626 (2010).
35. Bakurin, K. I. et al. Opponent regulation of action performance and timing by striatonigral and striatopallidal pathways. *eLife* **9**, e54831 (2020).
36. Tecuapetla, F., Matias, S., Dugue, G. P., Mainen, Z. F. & Costa, R. M. Balanced activity in basal ganglia projection pathways is critical for contraversive movements. *Nat. Commun.* **5**, 4315 (2014).
37. Freeze, B. S., Kravitz, A. V., Hammack, N., Berke, J. D. & Kreitzer, A. C. Control of basal ganglia output by direct and indirect pathway projection neurons. *J. Neurosci.* **33**, 18531–18539 (2013).
38. Rossi, M. A. et al. A wirelessly controlled implantable LED system for deep brain optogenetic stimulation. *Front. Integr. Neurosci.* **9**, 8 (2015).
39. Mathis, A. et al. DeepLabCut: markerless pose estimation of user-defined body parts with deep learning. *Nat. Neurosci.* **21**, 1281–1289 (2018).
40. Pisanello, F. et al. Dynamic illumination of spatially restricted or large brain volumes via a single tapered optical fiber. *Nat. Neurosci.* **20**, 1180–1188 (2017).
41. Ronzitti, E. et al. Recent advances in patterned photostimulation for optogenetics. *J. Opt.* **19**, 113001 (2017).
42. Forli, A. et al. Two-photon bidirectional control and imaging of neuronal excitability with high spatial resolution *in vivo*. *Cell Rep.* **22**, 3087–3098 (2018).
43. Kane, G. A., Lopes, G., Saunders, J. L., Mathis, A. & Mathis, M. W. Real-time, low-latency closed-loop feedback using markerless posture tracking. *eLife* **9**, e61909 (2020).
44. Zhou, P. et al. Efficient and accurate extraction of *in vivo* calcium signals from microendoscopic video data. *eLife* **7**, e28728 (2018).
45. Tran, L. M. et al. Automated curation of CNMF-E-extracted ROI spatial footprints and calcium traces using open-source AutoML tools. *Front. Neural Circuits* **14**, 42 (2020).

## Acknowledgements

We thank N. Calakos, S. Je and M. Rossi for helpful comments on the manuscript. This paper is dedicated to the memory of our co-author Ryan N. Hughes (1987–2021).

## Author contributions

H.H.Y. conceived the concept of the all-optical 1-photon system for freely moving mice. J.Z., N.K. and H.H.Y. designed the experiments. J.Z. designed, assembled and calibrated the circuit board and MAPSI. J.Z. and I.P.F performed testing in mice. J.Z., N.K. F.P. U.S. and K.B. analysed data. N.K., I.P.F., K.B. and R.N.H performed surgeries. R.N.H and J.K. performed histology and confocal imaging. R.N.H., J.Z. and H.H.Y. wrote the manuscript.

## Competing interests

H.H.Y. and J.Z. filed a provisional patent on the designs presented in this paper (63/289394, December 14, 2021, North Carolina, USA). The other authors declare no competing interests.

## Additional information

**Extended data** is available for this paper at <https://doi.org/10.1038/s41551-022-00920-3>.

**Supplementary information** The online version contains supplementary material available at <https://doi.org/10.1038/s41551-022-00920-3>.

**Correspondence and requests for materials** should be addressed to Henry H. Yin.

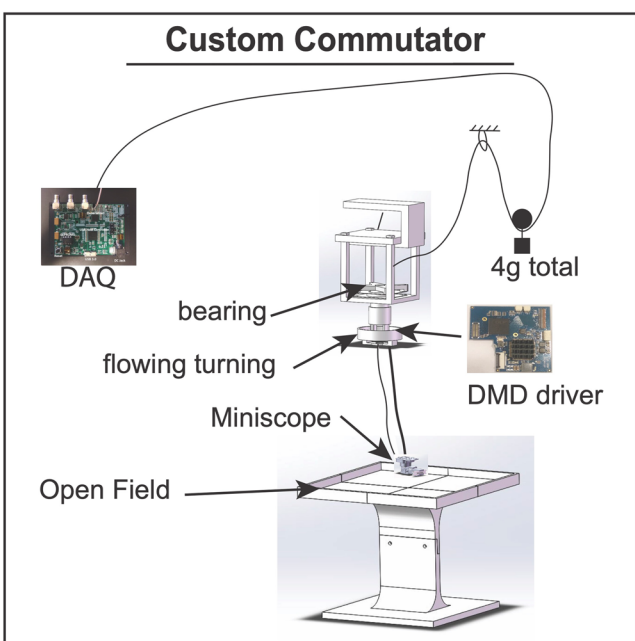
**Peer review information** *Nature Biomedical Engineering* thanks Dimitri Ryczko, Michael C. Wiest and the other, anonymous, reviewer(s) for their contribution to the peer review of this work.

**Reprints and permissions information** is available at [www.nature.com/reprints](http://www.nature.com/reprints).

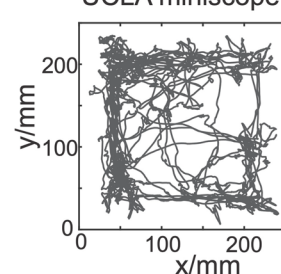
**Publisher's note** Springer Nature remains neutral with regard to jurisdictional claims in published maps and institutional affiliations.

Springer Nature or its licensor holds exclusive rights to this article under a publishing agreement with the author(s) or other rightsholder(s); author self-archiving of the accepted manuscript version of this article is solely governed by the terms of such publishing agreement and applicable law.

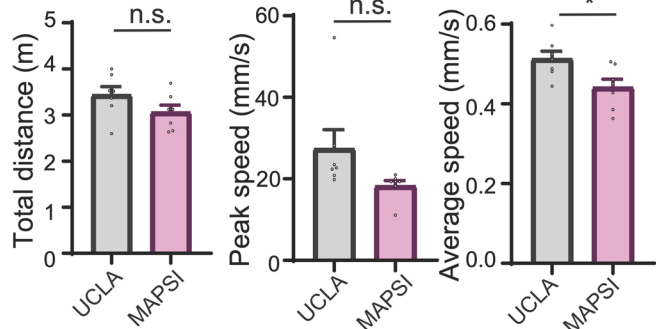
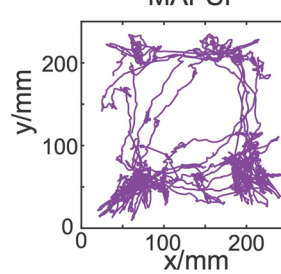
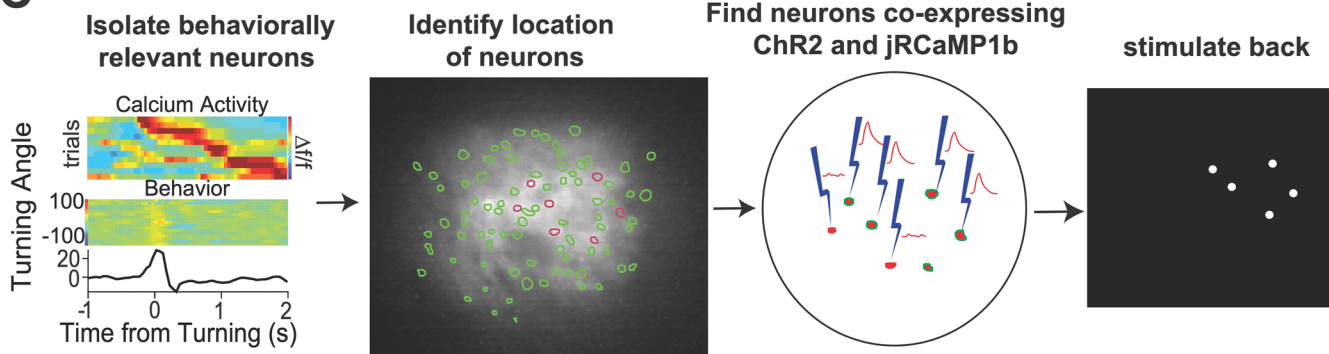
© The Author(s), under exclusive licence to Springer Nature Limited 2022

**A****B****15 minutes Free Behavior**

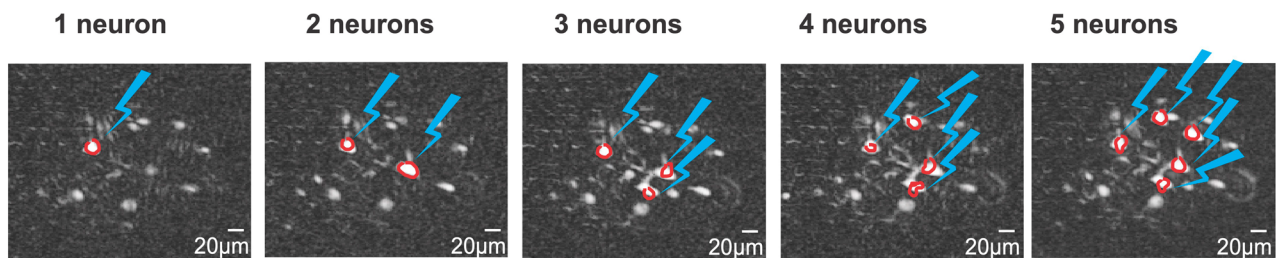
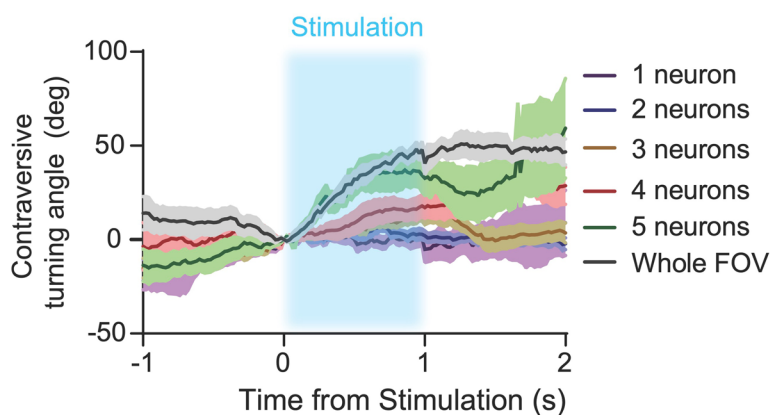
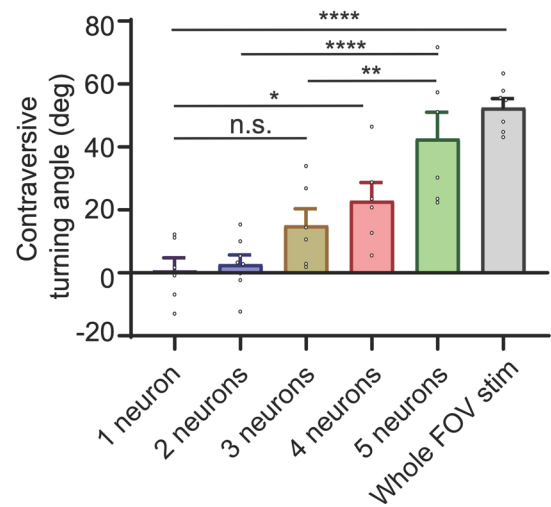
UCLA miniscope



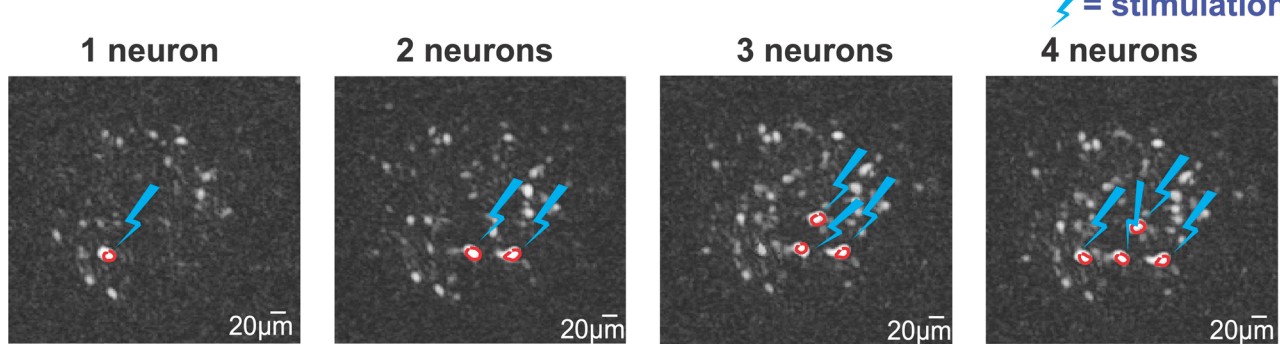
MAPSI

**Stimulation Pipeline****C**

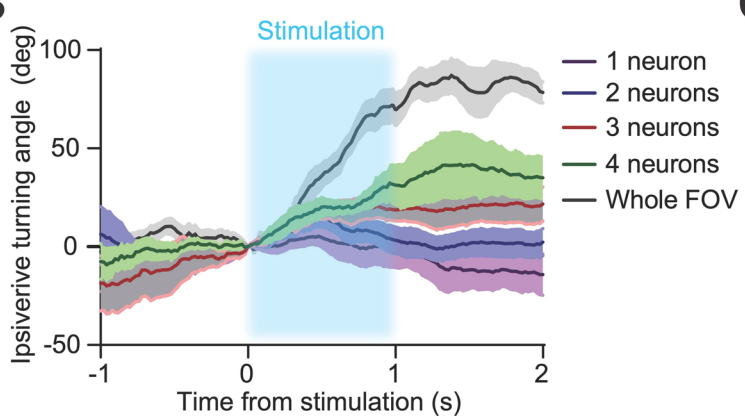
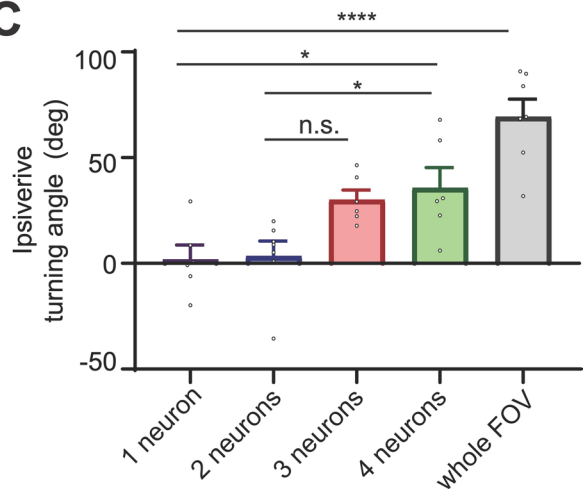
**Extended Data Fig. 1 | Free movement using MAPSI and stimulation pipeline.** To reduce the weight of MAPSI carried by the mouse, a custom commutator was built. **a**) The commutator is attached to a 4 g pulley, and allows the wires to rotate without being tangled. **b**) **Top:** Open field trajectory over 15 min of a representative mouse with 4 g UCLA miniscope compared to the trajectory of the same mouse carrying 7.8 g MAPSI. **Bottom:** Total movement distance, peak speed, and average speed ( $N=7$ , 4 D1-cre mice and 3 A2A-cre mice, 15 minutes in the same open field platform). Unpaired t test analysis revealed no significant difference between mice carrying UCLA Miniscope and MAPSI in distance ( $p=0.1274$ ) or peak speed ( $p=0.0826$ ), but mice carrying MAPSI showed reduced average speed ( $p=0.0238$ ). \*  $p < 0.05$ . **c**) Stimulation pipeline. Simultaneously record and analyze the calcium activity as well as the behavior. Isolate the behaviorally relevant neurons. Find the neurons that co-express both ChR2 and jRCaMP1b. Target neurons with co-expression and replay activity.

**A****B****C**

**Extended Data Fig. 2 | Contraversive turning behavior can be reliably elicited by stimulating as few as 3 dSPNs.** **a)** Calcium imaging of the selected direct pathway neurons for photostimulation. Anywhere from one to five neurons were selectively stimulated. **b)** Optogenetically stimulating 3 or more neurons reliably produced contraversive turning. **c)** Turning was significantly higher when exciting 3 or more neurons (One-way ANOVA,  $F_{(2,174)} = 15.39$ ,  $p = 0.0006$ ). Tukey's *post hoc* analysis revealed no significant difference between 2 neurons and 1 neuron ( $p = 0.9997$ ), no significant difference between 3 neurons and 1 neuron ( $p = 0.3750$ ), significant difference between 4 neurons and 1 neuron ( $p = 0.0454$ ), significant difference between 5 neurons and 1 neuron ( $p < 0.0001$ ), and significant difference between whole FOV stim and 1 neuron ( $p < 0.0001$ ). ( $N = 2$  D1-Cre mice, 15 trials for 1 neuron, 13 trials for 2 neurons, 13 trials for 3 neurons, 11 trials for 4 neurons, 19 trials for 5 neurons, and 14 trials for whole FOV). \*  $p < 0.05$ , \*\*  $p < 0.01$ , \*\*\*  $p < 0.001$ , \*\*\*\*  $p < 0.0001$ .

**A**

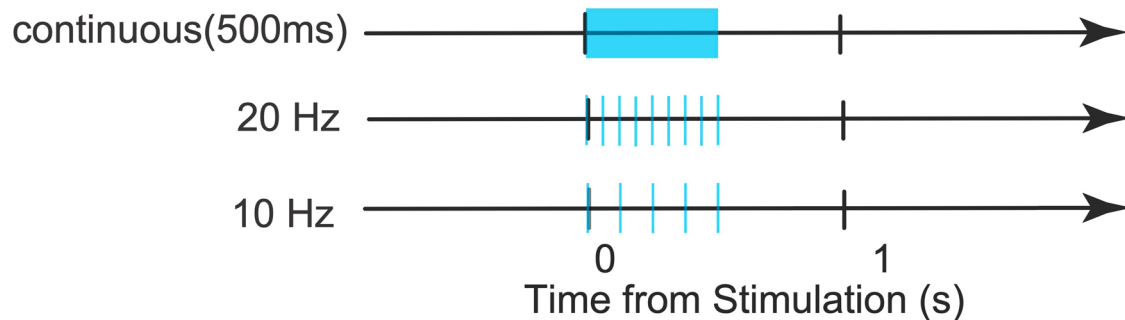
= stimulation

**B****C**

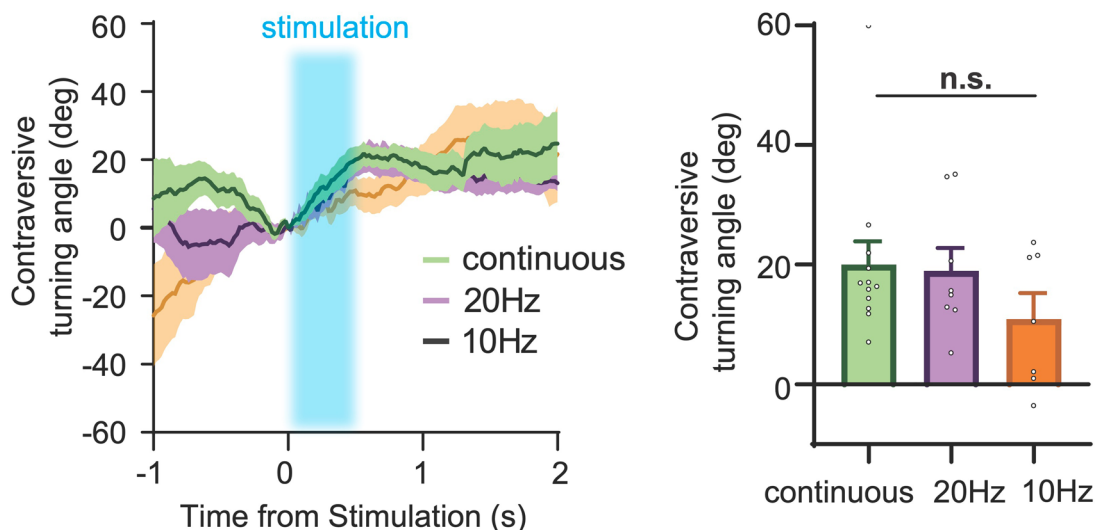
**Extended Data Fig. 3 | Ipsiversive turning behavior can be reliably elicited by stimulating as few as 3 iSPNs.** **a)** Images of the selected indirect pathway neurons for photostimulation. **b)** Stimulating 3 or more neurons reliably produced contraversive turning. **c)** Higher number of stimulated neurons increased maximum ipsiversive turning angle (One-way ANOVA,  $F_{(4,21)} = 6.104$ ,  $p = 0.0037$ ). Tukey's post hoc analysis revealed no significant difference between 2 neurons and 1 neuron ( $p = 0.9999$ ), no significant difference between 3 neurons and 1 neuron ( $p = 0.0953$ ), significant difference between 4 neurons and 1 neuron ( $p = 0.0303$ ), and significant difference between whole FOV stim and 1 neuron ( $p < 0.0001$ ). 2 A2A-Cre mice, 10 trials for 1 neuron, 7 trials for 2 neurons, 9 trials for 3 neurons, 13 trials for 4 neurons, and 11 trials for whole FOV.

**A**

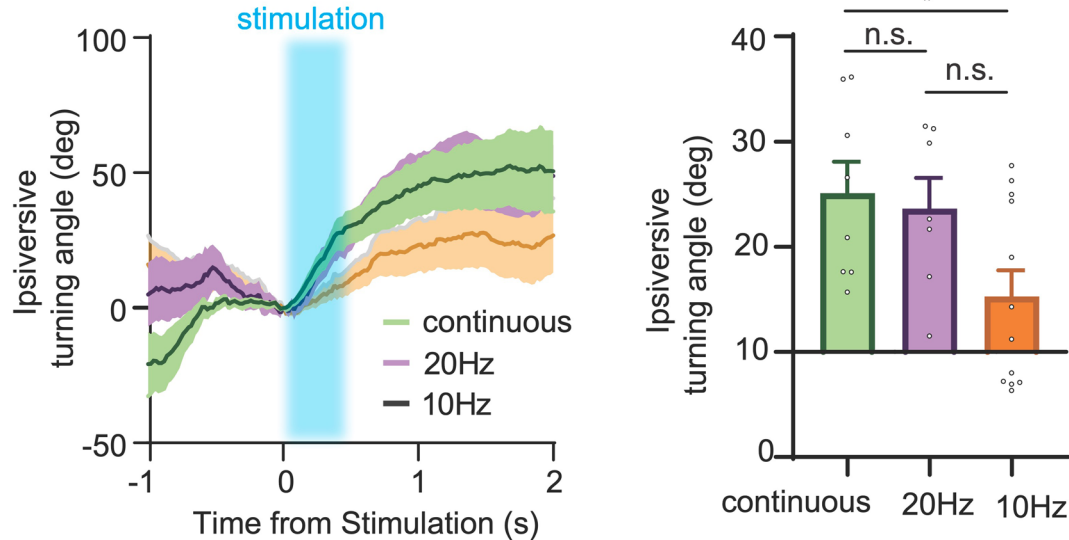
### Direct and Indirect pathway stimulation - different parameters of stimulation

**B**

### Direct pathway(*D1-Cre* mice)

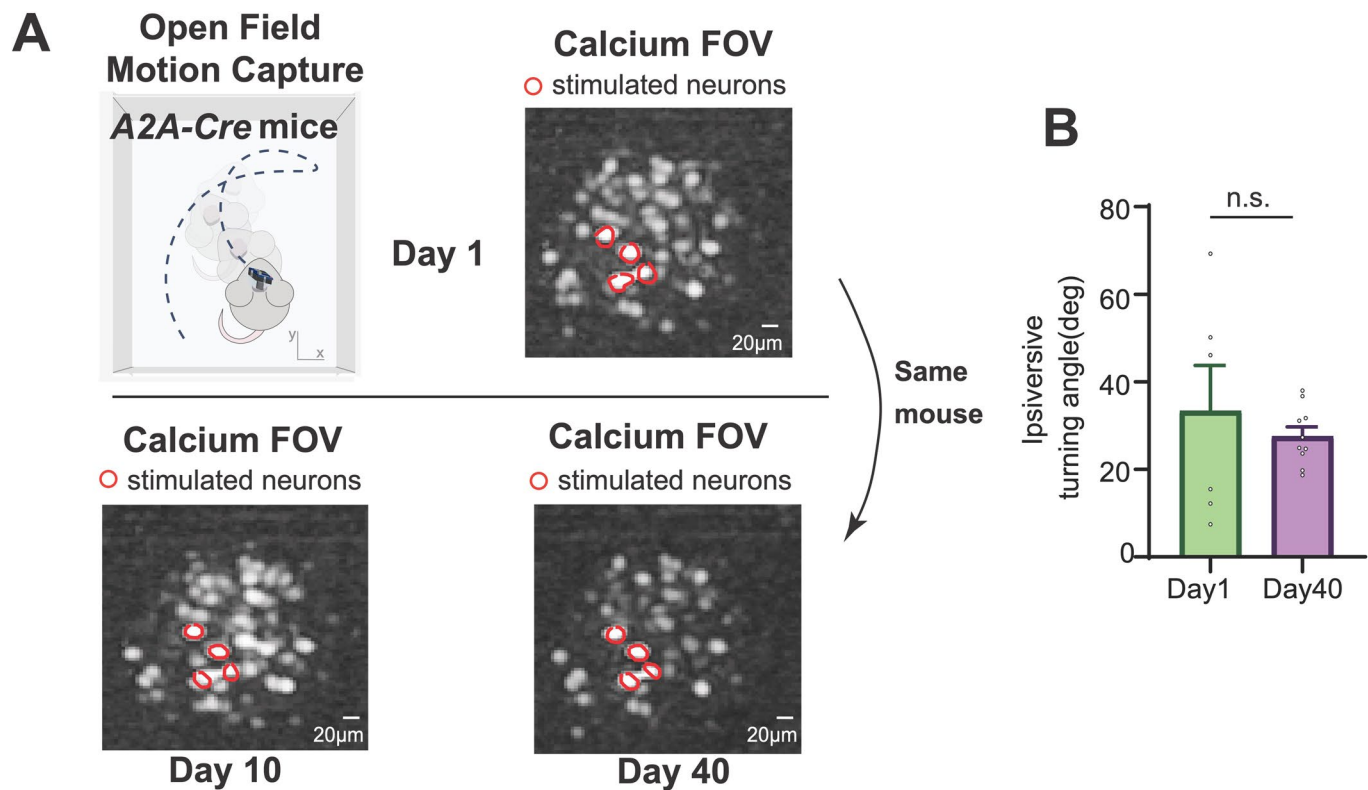
**C**

### Indirect pathway(*A2A-Cre* mice)



Extended Data Fig. 4 | See next page for caption.

**Extended Data Fig. 4 | There is no significant difference in turning from direct and indirect pathway stimulation using different parameters of stimulation.** **a)** We optogenetically stimulated neurons in the calcium imaging FOV with 3 different parameters: continuous 500 ms, 20 Hz (10 pulses in 500 ms), and 10 Hz (5 pulses in 500 ms). **b) Left**) Optogenetic excitation of direct pathway neurons in the DLS using the MAPSI significantly increased contraversive turning. **Right**) There was no significant stimulation effect (One-way ANOVA,  $F_{(2,24)}=1.315, p=0.2872$ ) ( $N=2$  *D1-cre* mice, 10 trials for 10 Hz, 8 trials for 20 Hz, and 12 trials for continuous). **c) Left**) Optogenetic excitation of indirect pathway neurons in the DLS using the MAPSI significantly increased ipsiversive turning behavior (One-way ANOVA,  $F_{(2,24)}=4.099, p=0.0294$ ; continuous vs 20 Hz,  $p=0.9367$ ; continuous vs 10 Hz,  $p=0.0407$ , 20 Hz vs 10 Hz,  $p=0.1080$ ) ( $2$  *A2A-cre* mice, 12 trials for 10 Hz, 8 trials for 20 Hz, and 8 trials for continuous). \*  $p<0.05$ .



**Extended Data Fig. 5 | Behavioral effect of stimulation is stable across time.** **a)** Top, a representative A2A-cre mouse was placed in an open field arena where several neurons were selected for stimulation on day 1 of a simultaneous stimulation and recording experiment. Shown on the right are the neurons selected for stimulation. Bottom, the same mouse was then tested 10 days and 40 days later in the open field arena, and the same neurons from day 1 were selectively stimulated. **b)** There was no significant difference in turning from day 1 compared to day 40 ( $t_{(14)} = 0.71, p = 0.49$ , 2 A2A-cre mice, 12 trials on day 1, 13 trials on day 40).

Corresponding author(s): Henry Yin

Last updated by author(s): Dec 4, 2021

## Reporting Summary

Nature Portfolio wishes to improve the reproducibility of the work that we publish. This form provides structure for consistency and transparency in reporting. For further information on Nature Portfolio policies, see our [Editorial Policies](#) and the [Editorial Policy Checklist](#).

### Statistics

For all statistical analyses, confirm that the following items are present in the figure legend, table legend, main text, or Methods section.

n/a Confirmed

- The exact sample size ( $n$ ) for each experimental group/condition, given as a discrete number and unit of measurement
- A statement on whether measurements were taken from distinct samples or whether the same sample was measured repeatedly
- The statistical test(s) used AND whether they are one- or two-sided  
*Only common tests should be described solely by name; describe more complex techniques in the Methods section.*
- A description of all covariates tested
- A description of any assumptions or corrections, such as tests of normality and adjustment for multiple comparisons
- A full description of the statistical parameters including central tendency (e.g. means) or other basic estimates (e.g. regression coefficient) AND variation (e.g. standard deviation) or associated estimates of uncertainty (e.g. confidence intervals)
- For null hypothesis testing, the test statistic (e.g.  $F$ ,  $t$ ,  $r$ ) with confidence intervals, effect sizes, degrees of freedom and  $P$  value noted  
*Give P values as exact values whenever suitable.*
- For Bayesian analysis, information on the choice of priors and Markov chain Monte Carlo settings
- For hierarchical and complex designs, identification of the appropriate level for tests and full reporting of outcomes
- Estimates of effect sizes (e.g. Cohen's  $d$ , Pearson's  $r$ ), indicating how they were calculated

*Our web collection on [statistics for biologists](#) contains articles on many of the points above.*

### Software and code

Policy information about [availability of computer code](#)

Data collection Data was collected using the UCLA Miniscope data acquisition software and Matlab.

Data analysis Data was analyzed using Matlab, Python, Graphpad Prism, and Neuroexplorer.

For manuscripts utilizing custom algorithms or software that are central to the research but not yet described in published literature, software must be made available to editors and reviewers. We strongly encourage code deposition in a community repository (e.g. GitHub). See the Nature Portfolio [guidelines for submitting code & software](#) for further information.

### Data

Policy information about [availability of data](#)

All manuscripts must include a [data availability statement](#). This statement should provide the following information, where applicable:

- Accession codes, unique identifiers, or web links for publicly available datasets
- A description of any restrictions on data availability
- For clinical datasets or third party data, please ensure that the statement adheres to our [policy](#)

The main data supporting the results in this study are available within the paper and its Supplementary Information. The raw and analysed datasets generated during the study are too large to be publicly shared, yet they are available for research purposes from the corresponding author on reasonable request.

# Field-specific reporting

Please select the one below that is the best fit for your research. If you are not sure, read the appropriate sections before making your selection.

Life sciences       Behavioural & social sciences       Ecological, evolutionary & environmental sciences

For a reference copy of the document with all sections, see [nature.com/documents/nr-reporting-summary-flat.pdf](https://nature.com/documents/nr-reporting-summary-flat.pdf)

## Life sciences study design

All studies must disclose on these points even when the disclosure is negative.

Sample size	Sample sizes were determined according to previous experience with calcium stimulation and imaging. No sample-size calculations were performed.
Data exclusions	No data were excluded.
Replication	The experiments were successfully replicated multiple times.
Randomization	Randomization was not necessary for this study, as the goal was simply to detect calcium signals and to measure the effects of stimulation.
Blinding	Blinding was not necessary for this study, as the goal was simply to detect calcium signals and to measure the effects of stimulation.

## Reporting for specific materials, systems and methods

We require information from authors about some types of materials, experimental systems and methods used in many studies. Here, indicate whether each material, system or method listed is relevant to your study. If you are not sure if a list item applies to your research, read the appropriate section before selecting a response.

Materials & experimental systems		Methods	
n/a	Involved in the study	n/a	Involved in the study
<input checked="" type="checkbox"/>	<input type="checkbox"/> Antibodies	<input checked="" type="checkbox"/>	<input type="checkbox"/> ChIP-seq
<input checked="" type="checkbox"/>	<input type="checkbox"/> Eukaryotic cell lines	<input checked="" type="checkbox"/>	<input type="checkbox"/> Flow cytometry
<input checked="" type="checkbox"/>	<input type="checkbox"/> Palaeontology and archaeology	<input checked="" type="checkbox"/>	<input type="checkbox"/> MRI-based neuroimaging
<input type="checkbox"/>	<input checked="" type="checkbox"/> Animals and other organisms		
<input checked="" type="checkbox"/>	<input type="checkbox"/> Human research participants		
<input checked="" type="checkbox"/>	<input type="checkbox"/> Clinical data		
<input checked="" type="checkbox"/>	<input type="checkbox"/> Dual use research of concern		

## Animals and other organisms

Policy information about [studies involving animals](#); [ARRIVE guidelines](#) recommended for reporting animal research

Laboratory animals	D1-Cre, A2A-Cre, wild-type mice.
Wild animals	The study did not involve wild animals.
Field-collected samples	The study did not involve samples collected from the field.
Ethics oversight	Duke IACUC committee.

Note that full information on the approval of the study protocol must also be provided in the manuscript.